An investigation on stiffness of a 3-PSP spatial parallel mechanism with flexible moving platform using invariant form

Amir Rezaei [a], Alireza Akbarzadeh [a,*], Mohammad-R. Akbarzadeh-T. [b]

[a] Center for Applied Research on Soft Computing and Intelligent Systems (CARSIS), ME Dept., Ferdowsi University of Mashhad, Mashhad, Iran
[b] Center for Applied Research on Soft Computing and Intelligent Systems (CARSIS), EE Dept., Ferdowsi University of Mashhad, Mashhad, Iran

ARTICLE INFO

ABSTRACT

In this paper, the stiffness of a 3-PSP spatial parallel manipulator is investigated. Unlike traditional stiffness analysis, the moving platform is assumed to be flexible. Two analytical methods are used in finding the robot stiffness. In the first method, robot is modeled as lumped system and principle of virtual work is used. In the second method, the robot is modeled as a distributed system and strain energy of robot main components as well as Castigliano's theorem are used. Force analysis is also presented and reaction forces at the joints as well as internal forces/moments are obtained. For each of the main robot components, a matrix called Wrench Compliant Module Jacobian, WCMJ, is introduced. These matrices will allow mapping the applied external wrench on the moving platform to corresponding reaction forces for the corresponding compliant module. All analysis is presented using invariant form. To evaluate accuracy of the two methods, finite element analysis is used. Finally, using the distributed method, maximum and minimum eigenvalues of the stiffness matrix are obtained and values of kinematic stiffness index are presented.

© 2011 Elsevier Ltd. All rights reserved.

1. Introduction

Application of parallel robots in industry continues to increase [1]. Some of these applications are simulators, machine tools, cutting and welding machines as well as CNC machines [2–5]. High precision and stiffness as well as good dynamic efficiency of parallel robots give them the capability to be used as CNC machines [5]. Earlier parallel robots usually have six degrees of freedom [6–8]. However, today, with increased application of parallel robots, robots with fewer numbers of degrees of freedom are needed [9,10]. These robots, in addition to having most of the capabilities of the parallel robots, can be made with less cost [11–13]. The economical factor of parallel robots with lower degrees of freedom has expanded their use in manufacturing processes [14,15]. In designing of parallel robots various criteria such as workspace, maximum capacity of load carrying, stiffness and KSI (kinematic stiffness index) should be investigated [16–20]. When parallel robots are used as machine tool, stiffness is considered one of the most important design parameters [4,15,21]. In fact, in parallel robots, accuracy has a direct relationship with stiffness of the robot. Accuracy and stiffness are two important parameters considered when designing machine tools [13,22]. Therefore, it is natural to consider use of inherently stiff parallel robots in machine tools and CNC machines. To study the stiffness of robots, two methods may be used to find the stiffness matrix of robot. The first method uses theoretical formulation while the second method uses actual experiments performed on robot [23]. Rezaei and Akbarzadeh [1] studied stiffness of a spatial parallel robot by considering flexibility effect of the moving platform using a distributed approach. Also, Enferadi and Akbarzadeh [24] investigated the stiffness of a spherical parallel robot by calculating strain energy of each component of the robot. However, in most studies, stiffness model of the parallel robots is considered as lumped. Li and Xu [22] derived the stiffness matrix of a 3-PUU PKM based on an alternative approach considering actuations and constraints. Kim and his coworkers

* Corresponding author. Tel.: +98 915 521 0253; fax: +98 511 876 3301.
E-mail addresses: amirrezaei_aico@yahoo.com (A. Rezaei), ali_akbarzadeh_t@yahoo.com (A. Akbarzadeh), akbarzadeh@ieee.org (M.-R. Akbarzadeh-T.).

investigated the stiffness analysis of a 3-DOF parallel robot with one constraining leg, which takes into account the elastic deformations of joints and links. To obtained stiffness matrix, overall Jacobian matrix and principle of virtual work are used [25].

The stiffness analysis of general 6-DOF parallel manipulators has been extensively reported, specifically, Stewart–Gough platform [26]. Gosselin used Jacobian matrix to study the stiffness of Stewart platform and the mapping between the driving force and the platform deformation [27]. To evaluate the robot stiffness variations throughout the workspace and to obtain the effect of altering the kinematics parameters in the structure, the eigenvalues of the stiffness matrix and KSI criteria are used [12,19,21,28]. In [20] a general and semi analytical approach for formulation of the stiffness matrix of parallel robot and its comparison with FEA is presented.

The purpose of stiffness analysis is to obtain its related stiffness matrix. Stiffness matrix relates 6 dimensional vector of small displacement for the end-effector and its corresponding 6 dimensional vector of applied static forces/torques (wrench). In robots, stiffness has a direct relationship with precision and maximum load carrying capacity [24]. It can be demonstrated that stiffness of a robot is limited between maximum and minimum eigenvalues of its stiffness matrix [12,22,28]. One method used to evaluate the stiffness is finding the maximum and minimum eigenvalues of the stiffness matrix and using KSI criterion [29]. Since the stiffness is a 6×6 matrix, 6 eigenvalues can be found. The stiffness of robot in its workspace can be evaluated by finding the maximum and minimum of its 6 eigenvalues throughout this space. For machine tool applications, the robot physical parameters should be designed so that the minimum values of the stiffness matrix, in its workspace, is greater than a desired value [3,22,19,28]. This will results in a desired accuracy for the machine. Therefore, determining low and high limits for stiffness of a robot is considered an essential part of a machine design [12,30].

In this paper, two analytical methods for solving the stiffness of 3-PSP parallel robot are presented. The presented methods are general and can be applied to most parallel robots. In the first method, stiffness of the robot is modeled as lumped and solved using principle of virtual work. In this method all flexible components such as, Linear rods and motors are modeled using linear springs. Jacobian analysis is first performed to find the relationship between displacement of the end-effector and the corresponding displacement of the actuators. Next, using principle of virtual work, the relationship between deformations of the end-effector and corresponding external wrench on the robot tip is obtained [13,22,25]. In the second method presented in this paper, unlike the first, stiffness of the robot is modeled as distributed system. This method is based on Castigliano's theorem and calculation of strain energy of the robot components. Traditional methods used for calculation of the robot stiffness, are based on modeling of stiffness as lumped. There are many limitations and assumptions used for simplification of the lumped model. However, when the robot is modeled as distributed system, there is no need to use any of the simplifying assumptions. Therefore, this method will be more accurate in modeling the stiffness. Furthermore, this method allows us to model the star shaped moving platform as a flexible body and include the effect of bending in all components of the robot. The results of the two methods, virtual work and Castigliano's, are further compared with results from a commercial finite element analysis software.

This paper is organized as follows: In Section 2, structure of a spatial 3-PSP parallel robot is introduced and solution to inverse kinematics of the robot is presented. In Section 3, a lumped stiffness model is presented using principle of virtual work. Next, the second method is presented for solving robot stiffness based on Castigliano's theorem. Calculation of the strain energy for the robot components assuming continuous model for the robot are presented. In Sections 4 and 5, the results of the two previous models are each compared with results from the FEA model. The method with higher accuracy is used for the subsequent analysis. In Section 6, the more accurate method is selected and the robot stiffness, using maximum and minimum eigenvalues of stiffness matrix, in its workspace is evaluated. The kinematic stiffness index (KSI) is also calculated for several sections of the workspace.

2. Structural description and inverse kinematics analysis

In this paper, a special type of 3-PSP parallel robot is investigated. The solid and physical models of a 3-PSP parallel manipulator are illustrated in Fig. 1(a) and (b). This robot is a fully parallel mechanism with three degree of freedom. This robot is composed of a moving platform which is shaped like a star and two fixed platforms. Selected tools may be placed in the center of the moving platform also referred to as moving star (MS). The moving star and the fixed platforms are connected together with three parallel legs with identical serial kinematic chains. Each of the three legs, consists of an active prismatic joint (P-joint), actuated by a Linear rod (LR), and a passive spherical joint (S-joint), followed by a second passive prismatic joint. Therefore, the MS is attached to the base by three identical serial PSP linkages. The three independent DOFs for the robot may be selected among the six possible degrees of freedoms (x, y, z, θ, φ and λ). In the present paper, two rotational and one translational variables θ, φ and z are selected as inputs for the inverse kinematics problem (see [2] for more details). Fig. 1(c) shows geometry for one of the three kinematic chains.

The vectors and reference frames are also described in this figure. A fixed coordinate frame B{x, y, z} is arbitrarily embedded in the top fixed platform and attached to the center point O of fixed triangle $\Delta A_1 A_2 A_3$. Likewise a moving coordinate frame T{u, v, w} is attached to the tool, at point T. In this paper, vectors referenced in fixed base coordinate frame {B} are denoted by $^B\mathbf{v}$, while vectors referenced in moving coordinate frame {T} are denoted by $^T\mathbf{v}$. The three spherical joints are denoted by S_i. Three position vectors $^B\mathbf{q}_i$, defined in {B}, connect corners of the fixed triangle, A_i, to the center of the spherical joints, S_i. Position of the end-effector (point T) with respect to {B} is given by vector $^B T$. Three additional position vectors, $^B\mathbf{a}_i$ locate corners of the fixed base, A_i, in {B}. The position vector $^T\mathbf{b}_i$, connects the end-effector, point T, to the *i*th spherical joint, S_i, and is defined in {T}.

Consider Fig. 1(c). Three closed vector-loop equations can be written as,

$$^B\mathbf{a}_i + {}^B\mathbf{q}_i = {}^B_T\mathbf{R} \, {}^T\mathbf{b}_i + {}^B\mathbf{T} \text{ for } i = 1, 2, 3 \tag{1}$$
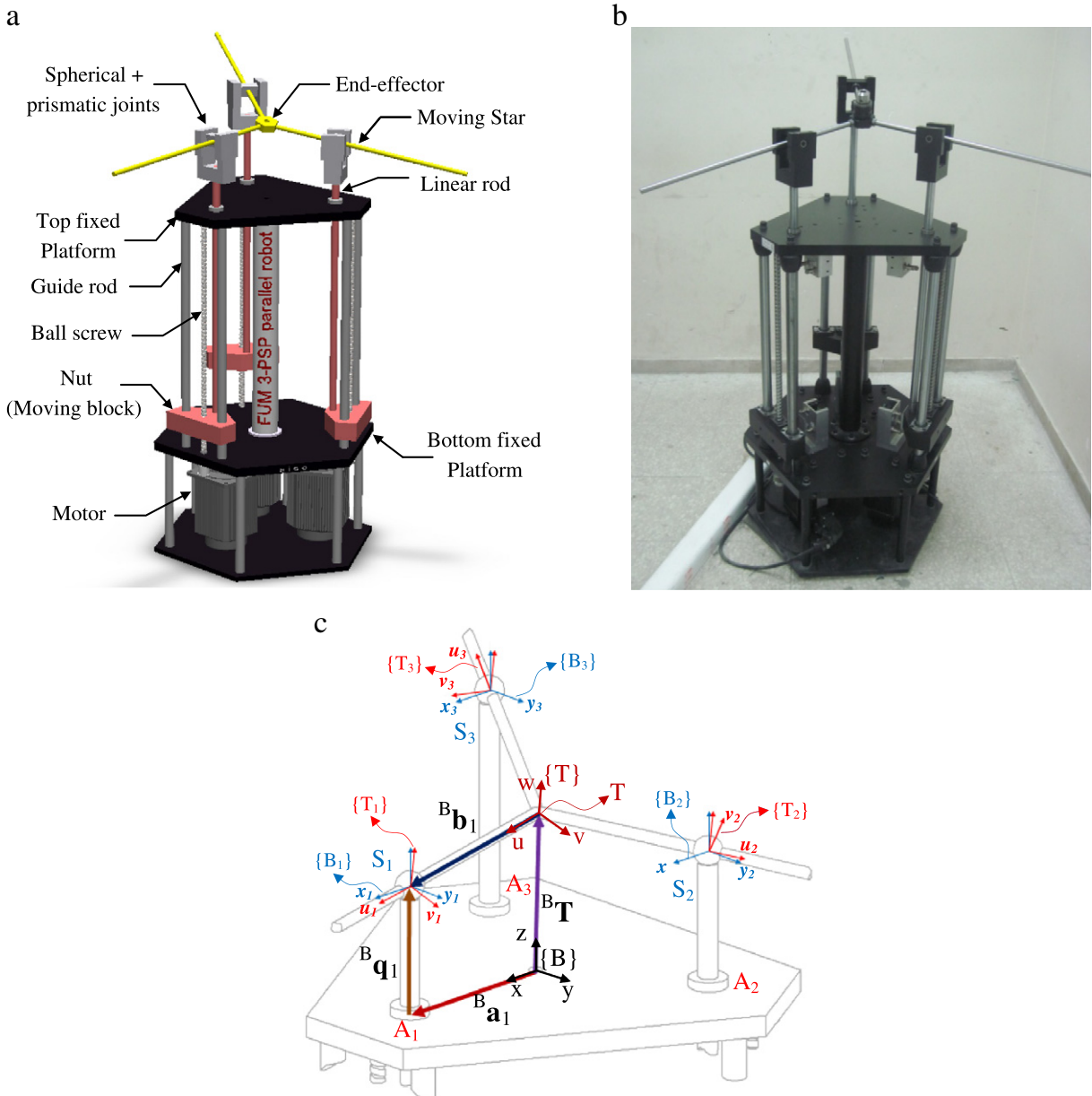
Fig. 1. (a) Solid model (b) physical model and (c) geometry of one kinematic chain of the 3-PSP parallel robot.

In inverse kinematics problem, a position vector for end-effector is given and vector specifying positions of actuators are deter-mined. Therefore, upon specifying position vector of the end-effector,^{B}**T**, the constraint equations, Eq. (1), can be solved. Therefore, kinematic values of robot which are necessary for Jacobian and stiffness analysis are obtained (see [2] for more details).

3. Stiffness analysis of 3-PSP parallel robot

In this paper, stiffness analysis of a 3-PSP parallel manipulator is presented. Stiffness analysis measures small deflection of robot's end-effector when external wrench is applied to this point. This relationship is expressed by stiffness matrix. Before obtaining the stiffness matrix, we must first find the relationship between applied external wrench on MS and the resultant joints forces. From forced analysis, several analytical expressions will be obtained. These analytical expressions will allow us to calculate reaction forces for all 3-PSP manipulator configurations. To do this, the robot is considered to be comprised of three compliant modules. First compliant module is the moving star. The second and third compliant modules are the linear rods and the motors, respectively. In this paper, force analysis is performed for all three compliant modules. This is performed by introducing the

Wrench Compliant Module Jacobian, WCMJ, matrices. These matrices will allow us to map the applied external wrench on MS to corresponding reaction forces for that compliant module.

Most present methods used to find robot stiffness matrix use lumped model. The existing limitations in these methods require a series of simplifying assumptions used in the process of modeling robot stiffness. The most important of these assumptions is that the moving platform is assumed to be rigid. Also most articles do not consider the effect of bending of robot members.

In this paper, two methods for obtaining robot stiffness matrix are presented. In the first method, principle of virtual work is used. The MS is assumed to be rigid and bending in all components of the robot is assumed to be negligible. In the second method, unlike traditional stiffness modeling methods, the MS is modeled as flexible. Furthermore, bending in all components of the robot is considered. To do this, a continuous method is used for obtaining the manipulator stiffness matrix. This method is based on strain energy and Castigliano's theorem. To obtain strain energy of all components, first, inverse kinematic and forced analysis must be performed. Next, using Castigliano's theorem, stiffness matrix that maps small displacement of the end-effector to applied external wrench, is obtained.

3.1. Lumped modeling of stiffness matrix

In this subsection, the development of stiffness matrix for 3-PSP parallel robot is presented based on principle of virtual work. To use a lumped model, the following assumptions must be made,

- The MS is assumed to be rigid.
- Bending in all compliant modules (MS, LR) is assumed to be negligible.
- Weights of all compliant modules of the robot are negligible.
- Passive joints are assumed to be rigid and all joints are frictionless.
- Rigidities of the ball screws and guide rods are infinite.
- Motors, linear rods are assumed flexible

3.1.1. Obtaining equivalent stiffness for motors and Linear rods

The moving platform is supported by a total of six springs, in which three springs are related to the linear rods and the other three are related to the motors. The values of spring constants are determined by modeling the compliances in each leg. As shown in Fig. 2, K_{ai} is equivalent stiffness value of the *i*th LR and is equal to A_bE_b/q_i. Additionally, stiffness for the *i*th motor, K_{mi}, is modeled by a equivalent linear spring. To obtain the value of q_i, in different robot configurations, the inverse position analysis must be completed. First, consider the reaction forces on S-joints are due to shear and axial forces at the end of LRs. The axial force will result in a moment on the motor. The moment will further result in a rotational deformation on motor shaft. The rotational deformation in motor will result in a linear displacement of the moving block along the z-direction.

The equivalent torsional stiffness of motor and applied moment on motor are denoted by K_{tor} and τ_m, respectively. Then, rotational deformation of motor, $\Delta\theta_m$, is expressed as,

$$\Delta\theta_m = \tau_m/K_{tor} \tag{2}$$

Also, the relationship between linear displacement of the nut,Δq, and rotational deformation of motor is represented by,

$$\Delta q = \left(\frac{Nl_b}{2\pi}\right)\Delta\theta_m \tag{3}$$
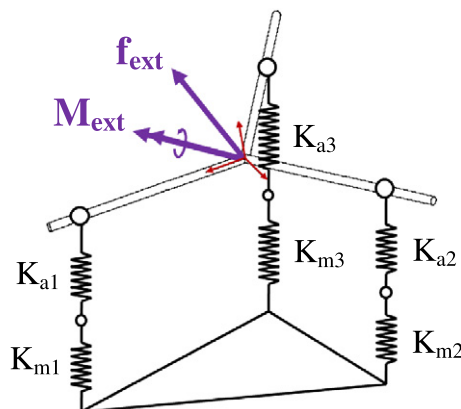
Fig. 2. Lumped model of a 3-PSP parallel robot.

Where, l_b is the lead of the ball screw and N represents the gearbox transmission ratio. Also, the relationship between axial reaction force, f on LR and applied moment on motor due to gearbox transmission ratio is represented as,

$$f = \frac{2\pi}{Nl_b}\tau_m \tag{4}$$

Using Eqs.(3) and (4), equivalent linear spring which models the stiffness of the ith motor can be determined. Since all three motors are assumed to be equal, we can write,

$$K_m = \frac{f}{\Delta q} = \left(\frac{2\pi}{Nl_b}\right)^2 K_{tor} \tag{5}$$

3.1.2. Determination of stiffness matrix

The overall Jacobian matrix of robot is a matrix that expresses the relationship between velocities in Cartesian space and velocities in joint space of a manipulator. The velocity relation for the 3-PSP parallel robot is written as (see [2] for more details),

$$\dot{\mathbf{q}} = \mathbf{J}\mathbf{t} \tag{6}$$

Where $\mathbf{J}$ is a 3×6 matrix called overall Jacobian matrix of the 3-PSP parallel manipulator. Let $\dot{\mathbf{q}} = [\dot{q}_1 \quad \dot{q}_2 \quad \dot{q}_3]^T$ and $\mathbf{t} = [\mathbf{v}_P \quad \omega_s]^T$ be the vectors of the linear actuated joint rates and the MS velocities, respectively. Where $\mathbf{v}_P = [\dot{x} \quad \dot{y} \quad \dot{z}]^T$ and $\omega_s = [\dot{\theta} \quad \dot{\varphi} \quad \dot{\lambda}]^T$, represent translational and angular velocities of MS, respectively. Considering Eq. (6), we can write,

$$\delta\mathbf{q} = \mathbf{J}\delta\mathbf{S} \tag{7}$$

Where, $\delta\mathbf{q}$ is virtual infinitesimal displacement vector of LRs and $\delta\mathbf{S}$ is virtual infinitesimal twist vector of the end-effector. According to the principle of virtual work, we have

$$\mathbf{W}^T\delta\mathbf{S} = \tau^T\delta\mathbf{q} \tag{8}$$

Where, τ is the vector of applied forces at the actuated joints and $\mathbf{W}$ is the vector of applied external wrench at the end-effector. According to the Hook's law, the relation between virtual infinitesimal displacement vector of LRs and vector of applied forces at the actuated joints can be written as,

$$\tau = \kappa_a\delta\mathbf{q} \tag{9}$$

Where, κ_a is a diagonal matrix consisting of stiffness of the motors, represented by linear spring, and the equivalent stiffness of LRs. This matrix can be defined as,

$$\kappa_a = \text{diag}\left(K_{eq1}, K_{eq2}, K_{eq3}\right) \tag{10}$$

As shown Fig. 2, we know that the two equivalents springs K_{mi} and K_{ai} are in series with each other. Then, total equivalent spring for each robot leg can be obtained as follows,

$$K_{eqi} = \frac{K_{ai}K_{mi}}{K_{ai} + K_{mi}} \qquad \text{for } i = 1, 2, 3 \tag{11}$$

Substituting Eq.(9) into Eq.(8) yields,

$$\mathbf{W}^T\delta\mathbf{S} = \delta\mathbf{q}^T\kappa_a\delta\mathbf{q} \tag{12}$$

Considering Eq. (7), we have,

$$\mathbf{W}^T\delta\mathbf{S} = \delta\mathbf{S}^T\left(\mathbf{J}^T\kappa_a\mathbf{J}\right)\delta\mathbf{S} \tag{13}$$

Finally, Eq. (13) can be written as follows,

$$\mathbf{W} = \mathbf{K}\delta\mathbf{S} \tag{14}$$

Where, $\delta\mathbf{S} = [\delta\boldsymbol{\chi} \quad \delta\boldsymbol{\psi}]^T$ consists of $\delta\boldsymbol{\chi} = [\delta x \quad \delta y \quad \delta z]^T$ a translational displacement vector of MS center and $\delta\boldsymbol{\psi} = [\delta\theta \quad \delta\varphi \quad \delta\lambda]^T$ a rotational displacement vector of MS center. Matrix $\mathbf{K}$ is called overall stiffness matrix of the 3-PSP parallel robot. Using Eqs. (13) and (14), the overall stiffness matrix is obtained by,

$$\mathbf{K} = \mathbf{J}^T\kappa_a\mathbf{J} \tag{15}$$

3.2. Distributed modeling of stiffness matrix

In this subsection, the development of stiffness matrix for 3-PSP parallel robot is presented based on Castigliano's theorem and strain energy. The following assumptions are made,

- The MS is assumed to be flexible
- Bending in all compliant modules (MS, LR, and Motors) is considered.
- Weights of all compliant modules are negligible.
- Passive joints are assumed to be rigid
- All joints are frictionless.
- Strain energy due to shear forces is negligible.

We presume that the listed assumptions result in stiffness modeling that is very realistic and should closely approximate the stiffness of the actual robotic manipulator.

3.2.1. Determination of compliance matrix of robot's modules and force analysis

In this subsection, strain energy of all compliant modules of the 3-PSP parallel robot is calculated. For this purpose, force analysis and inverse position analysis will be used. Generally, total strain energy of manipulator can be written as,

$$U = U_{MS} + U_{LR} + U_M \tag{16}$$

Where, U_{MS} is strain energy of MS, U_{LR} is strain energy of the three LRs and U_M is strain energy of the three motors. The overall stiffness matrix, $\mathbf{K}$, is the mapping between applied external wrench and infinitesimal twist (rotational and translational displacement) at the end-effector. Therefore, using Hooke's law, this mapping for the whole robot structure can be written as,

$$\mathbf{W} = \mathbf{K}\delta\mathbf{S} \tag{17}$$

Where $\mathbf{W}$ and $\delta\mathbf{S}$ represent, external wrench applied to the center of MS and virtual twist of the MS center, respectively. $\delta\mathbf{S}$ contains virtual translation, $\delta\boldsymbol{\chi}$, and virtual rotation, $\delta\boldsymbol{\psi}$, vector of MS center. Hence,

$$\delta\mathbf{S} = [\begin{array}{cccccc} \delta x & \delta y & \delta z & \delta\theta & \delta\varphi & \delta\lambda \end{array}]^T = [\begin{array}{cc} \delta\boldsymbol{\chi} & \delta\boldsymbol{\psi} \end{array}]^T \tag{18}$$

Using Castigliano's theorem, we can obtain overall virtual twist vector of MS as follow,

$$\delta\boldsymbol{\chi} = \frac{\partial U}{\partial \mathbf{f}_{ext}} = \frac{\partial U_{MS}}{\partial \mathbf{f}_{ext}} + \frac{\partial U_{LR}}{\partial \mathbf{f}_{ext}} + \frac{\partial U_M}{\partial \mathbf{f}_{ext}} = \delta\boldsymbol{\chi}_{MS} + \delta\boldsymbol{\chi}_{LR} + \delta\boldsymbol{\chi}_M \tag{19}$$

$$\delta\boldsymbol{\psi} = \frac{\partial U}{\partial \mathbf{M}_{ext}} = \frac{\partial U_{MS}}{\partial \mathbf{M}_{ext}} + \frac{\partial U_{LR}}{\partial \mathbf{M}_{ext}} + \frac{\partial U_M}{\partial \mathbf{M}_{ext}} = \delta\boldsymbol{\psi}_{MS} + \delta\boldsymbol{\psi}_{LR} + \delta\boldsymbol{\psi}_M \tag{20}$$

Therefore, the virtual twist vectors due to flexibility of MS, LRs and motors can be written as,

$$\delta\mathbf{S}_{MS} = [\begin{array}{cc} \delta\boldsymbol{\chi}_{MS} & \delta\boldsymbol{\psi}_{MS} \end{array}]^T = [\begin{array}{cccccc} \delta\chi_{MSx} & \delta\chi_{MSy} & \delta\chi_{MSz} & \delta\psi_{MSx} & \delta\psi_{MSy} & \delta\psi_{MSz} \end{array}]^T = \mathbf{C}_{MS}\mathbf{W} \tag{21}$$

$$\delta\mathbf{S}_{LR} = [\begin{array}{cc} \delta\boldsymbol{\chi}_{LR} & \delta\boldsymbol{\psi}_{LR} \end{array}]^T = [\begin{array}{cccccc} \delta\chi_{LRx} & \delta\chi_{LRy} & \delta\chi_{LRz} & \delta\psi_{LRx} & \delta\psi_{LRy} & \delta\psi_{LRz} \end{array}]^T = \mathbf{C}_{LR}\mathbf{W} \tag{22}$$

$$\delta\mathbf{S}_M = [\begin{array}{cc} \delta\boldsymbol{\chi}_M & \delta\boldsymbol{\psi}_M \end{array}]^T = [\begin{array}{cccccc} \delta\chi_{Mx} & \delta\chi_{My} & \delta\chi_{Mz} & \delta\psi_{Mx} & \delta\psi_{My} & \delta\psi_{Mz} \end{array}]^T = \mathbf{C}_M\mathbf{W} \tag{23}$$

Where $\mathbf{C}_{MS}$, $\mathbf{C}_{LR}$ and $\mathbf{C}_M$ are compliance matrices of the MS, LRs and motors, respectively. Therefore, the virtual twist vector of the MS center, point T on end-effector, can be written as,

$$\delta\mathbf{S} = \delta\mathbf{S}_{MS} + \delta\mathbf{S}_{LR} + \delta\mathbf{S}_M = (\mathbf{C}_{MS} + \mathbf{C}_{LR} + \mathbf{C}_M)\mathbf{W} = \mathbf{C}_{6\times6}\mathbf{W} \tag{24}$$

Where $\mathbf{C}$ is the overall compliance matrix of the 3-PSP robot. Eq. (17) can be rewritten as,

$$\mathbf{W} = \mathbf{C}^{-1}\delta\mathbf{S} \tag{25}$$

Comparing Eqs. (17) and (25), the stiffness matrix for the 3-PSP parallel robot can be obtained as,

$$\mathbf{K} = \mathbf{C}^{-1} \tag{26}$$

Next, the compliance related to all robot compliant modules must be determined. To do this, first force analysis for each compliant module should be performed. The force analysis is presented by introducing the Wrench Compliant Module Jacobian matrices, WCMJ.

3.2.1.1. Compliance matrix of moving star (MS). In this subsection, first the relationship between the applied external wrench on the end-effector, point T, and the resultant joints forces is determined. Assume that the MS experiences an external wrench $^B\mathbf{W}$ defined in the fixed coordinate {B} as follow,

$$^B\mathbf{W}_{6\times1} = \begin{bmatrix} ^B\mathbf{f}_{ext} & ^B\mathbf{M}_{ext} \end{bmatrix}^T \quad , \quad ^B\mathbf{f}_{ext} = \begin{bmatrix} f_x & f_y & f_z \end{bmatrix}^T \quad , \quad ^B\mathbf{M}_{ext} = \begin{bmatrix} M_x & M_y & M_z \end{bmatrix}^T \tag{27}$$

Where $^B\mathbf{f}_{ext}$ denotes a force vector and $^B\mathbf{M}_{ext}$ denotes a moment vector in {B}. As shown in Fig. 3, $^T\mathbf{F}$ is a vector of reaction forces between the ith prismatic passive joint and ith branch of MS in{T}. We also define three additional frames {T_i} which are attached to the S-joints with their x-axis long the $\mathbf{b}_i$ vectors. The overall vector of reaction forces is expressed as

$$^T\mathbf{F}_{6\times1} = \begin{bmatrix} f_{v1} & f_{w1} & f_{v2} & f_{w2} & f_{v3} & f_{w3} \end{bmatrix}^T \tag{28}$$

Where f_{vi}, f_{wi} are values of reaction forces in ith prismatic passive joint.

For a given configuration of 3-PSP manipulator, directions of all unit vectors are determined by inverse kinematics problem. The relation between these forces and applied external wrench on MS may be written as,

$$\mathbf{F} = \sum_{i=1}^{3} {}^B_{Ti}\mathbf{R} \left(f_{vi}{}^{Ti}\mathbf{v}_i + f_{wi}{}^{Ti}\mathbf{w}_i \right) + {}^B\mathbf{f}_{ext} = 0 \tag{29}$$

$$\mathbf{M}_T = \sum_{i=1}^{3} {}^B_{Ti}\mathbf{R} \left(b_i f_{vi} \left({}^{Ti}\mathbf{b}_i \times {}^{Ti}\mathbf{v}_i \right) + b_i f_{wi} \left({}^{Ti}\mathbf{b}_i \times {}^{Ti}\mathbf{w}_i \right) \right) + {}^B\mathbf{M}_{ext} = 0 \tag{30}$$

Where, $^{Ti}\mathbf{v}_i$, $^{Ti}\mathbf{w}_i$ are unit vectors along the reaction forces in {T_i} and $^{Ti}\mathbf{b}_i$ denote unit vectors along each branch of MS in {T_i}. By simplifying above equations, we obtain a relation between external wrench and reaction forces in matrix form as,

$$\mathbf{W}_{6\times1} + \mathbf{A}_{6\times6}{}^T\mathbf{F}_{6\times1} = 0 \tag{31}$$

Eq. (31) can be rewritten as,

$$^T\mathbf{F}_{6\times1} = \mathbf{B}_{6\times6}\mathbf{W}_{6\times1} \quad \rightarrow \quad \mathbf{B} = -\mathbf{A}^{-1} \tag{32}$$

Matrix **B** is called Wrench Compliant Module Jacobian, WCMJ$_{MS}$, matrix for MS. Note, this matrix maps the applied external wrench on MS to corresponding reaction forces for the compliant module under study, in this case, the MS. The components of
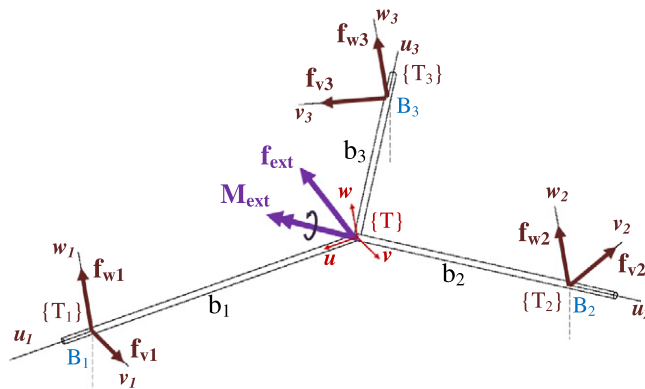
Fig. 3. Free body diagram (FBD) of the moving star (MS).
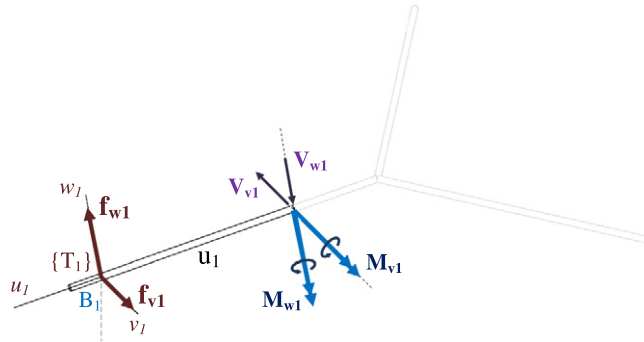
Fig. 4. FBD and section view of the ith branch of the MS.

the **B** matrix are referred to as b_{ij}. Next, to calculate the total strain energy of MS due to applied external wrench, the internal bending moment in each branch of MS should be calculated. Consider Fig. 4. We can write,

$$M_{vi} = f_{wi}u_i \qquad \text{for } i = 1, 2, 3 \tag{33}$$

$$M_{wi} = f_{vi}u_i \qquad \text{for } i = 1, 2, 3 \tag{34}$$

Strain energy of MS, U_{MS}, can be written as follows,

$$U_{MS} = \sum_{i=1}^{3} \int_{0}^{bi} \frac{1}{2EI} \left(M_{vi}^2 + M_{wi}^2 \right) du_i, \qquad 0 \leq u_i \leq b_i \tag{35}$$

Where b_i is the length of ith branch of MS. The value of b_i can be determined by solving the inverse kinematics problem at the desired robot configuration. Using Castigliano's theorem and Eq. (35), the virtual twist vector due to flexibility of the moving star, $\delta \mathbf{S}_{MS}$, can be expanded as follows,

i. Virtual translational displacement of MS, $\delta \boldsymbol{\chi}_{MS}$

$$\delta \chi_{MSx} = \frac{\partial U_{MS}}{\partial f_x} = \sum_{i=1}^{3} \int_{0}^{bi} \frac{1}{E_{MS}I_{MS}} \left(M_{vi} \frac{\partial M_{vi}}{\partial f_x} + M_{wi} \frac{\partial M_{wi}}{\partial f_x} \right) du_i \tag{36a}$$

$$\delta \chi_{MSy} = \frac{\partial U_{MS}}{\partial f_y} = \sum_{i=1}^{3} \int_{0}^{bi} \frac{1}{E_{MS}I_{MS}} \left(M_{vi} \frac{\partial M_{vi}}{\partial f_y} + M_{wi} \frac{\partial M_{wi}}{\partial f_y} \right) du_i \tag{36b}$$

$$\delta \chi_{MSz} = \frac{\partial U_{MS}}{\partial f_z} = \sum_{i=1}^{3} \int_{0}^{bi} \frac{1}{E_{MS}I_{MS}} \left(M_{vi} \frac{\partial M_{vi}}{\partial f_z} + M_{wi} \frac{\partial M_{wi}}{\partial f_z} \right) du_i \tag{36c}$$

ii. Virtual rotational displacement of MS, $\delta \boldsymbol{\psi}_{MS}$

$$\delta \psi_{MSx} = \frac{\partial U_{MS}}{\partial M_x} = \sum_{i=1}^{3} \int_{0}^{bi} \frac{1}{E_{MS}I_{MS}} \left(M_{vi} \frac{\partial M_{vi}}{\partial M_x} + M_{wi} \frac{\partial M_{wi}}{\partial M_x} \right) du_i \tag{37a}$$

$$\delta \psi_{MSy} = \frac{\partial U_{MS}}{\partial M_y} = \sum_{i=1}^{3} \int_{0}^{bi} \frac{1}{E_{MS}I_{MS}} \left(M_{vi} \frac{\partial M_{vi}}{\partial M_y} + M_{wi} \frac{\partial M_{wi}}{\partial M_y} \right) du_i \tag{37b}$$

$$\delta \psi_{MSz} = \frac{\partial U_{MS}}{\partial M_z} = \sum_{i=1}^{3} \int_{0}^{bi} \frac{1}{E_{MS}I_{MS}} \left(M_{vi} \frac{\partial M_{vi}}{\partial M_z} + M_{wi} \frac{\partial M_{wi}}{\partial M_z} \right) du_i \tag{37c}$$

Where $\delta \mathbf{S}_{MS} = \begin{bmatrix} \delta\chi_{MSx} & \delta\chi_{MSy} & \delta\chi_{MSz} & \delta\psi_{MSx} & \delta\psi_{MSy} & \delta\psi_{MSz} \end{bmatrix}^T$ is a 6×1 vector. Where, $\delta\chi_{MSx}$, $\delta\chi_{MSy}$ and $\delta\chi_{MSz}$ are components of virtual translational displacement and $\delta\psi_{MSx}$, $\delta\psi_{MSy}$ and $\delta\psi_{MSz}$ are components of virtual rotational displacement about x-, y- and z- axes in fixed coordinate frame {B}. The components of **B** matrix, Eq. (32), are substituted into Eqs. (33–34). Results are placed into

the above equations, Eqs. (36a–c)–(37a–c), and next integrated. Finally, external applied wrench, **W**, is factored which provides the virtual twist vector due to flexibility of MS in terms of applied external wrench. For $j = 1, 2, \cdots, 6$, we can write

$$\delta \chi_{MSx} = \frac{1}{3E_{MS}I_{MS}} \left(\left(b_{11}\mathbf{b}_{1j} + b_{21}\mathbf{b}_{2j} \right) b_1^3 + \left(b_{31}\mathbf{b}_{3j} + b_{41}\mathbf{b}_{4j} \right) b_2^3 + \left(b_{51}\mathbf{b}_{5j} + b_{61}\mathbf{b}_{6j} \right) b_3^3 \right) \mathbf{W} \tag{38a}$$

$$\delta \chi_{MSy} = \frac{1}{3E_{MS}I_{MS}} \left(\left(b_{12}\mathbf{b}_{1j} + b_{22}\mathbf{b}_{2j} \right) b_1^3 + \left(b_{32}\mathbf{b}_{3j} + b_{42}\mathbf{b}_{4j} \right) b_2^3 + \left(b_{52}\mathbf{b}_{5j} + b_{62}\mathbf{b}_{6j} \right) b_3^3 \right) \mathbf{W} \tag{38b}$$

$$\delta \chi_{MSz} = \frac{1}{3E_{MS}I_{MS}} \left(\left(b_{13}\mathbf{b}_{1j} + b_{23}\mathbf{b}_{2j} \right) b_1^3 + \left(b_{33}\mathbf{b}_{3j} + b_{43}\mathbf{b}_{4j} \right) b_2^3 + \left(b_{53}\mathbf{b}_{5j} + b_{63}\mathbf{b}_{6j} \right) b_3^3 \right) \mathbf{W} \tag{38c}$$

and,

$$\delta \psi_{MSx} = \frac{1}{3E_{MS}I_{MS}} \left(\left(b_{14}\mathbf{b}_{1j} + b_{24}\mathbf{b}_{2j} \right) b_1^3 + \left(b_{34}\mathbf{b}_{3j} + b_{44}\mathbf{b}_{4j} \right) b_2^3 + \left(b_{54}\mathbf{b}_{5j} + b_{64}\mathbf{b}_{6j} \right) b_3^3 \right) \mathbf{W} \tag{39a}$$

$$\delta \psi_{MSy} = \frac{1}{3E_{MS}I_{MS}} \left(\left(b_{15}\mathbf{b}_{1j} + b_{25}\mathbf{b}_{2j} \right) b_1^3 + \left(b_{35}\mathbf{b}_{3j} + b_{45}\mathbf{b}_{4j} \right) b_2^3 + \left(b_{55}\mathbf{b}_{5j} + b_{65}\mathbf{b}_{6j} \right) b_3^3 \right) \mathbf{W} \tag{39b}$$

$$\delta \psi_{MSz} = \frac{1}{3E_{MS}I_{MS}} \left(\left(b_{16}\mathbf{b}_{1j} + b_{26}\mathbf{b}_{2j} \right) b_1^3 + \left(b_{36}\mathbf{b}_{3j} + b_{46}\mathbf{b}_{4j} \right) b_2^3 + \left(b_{56}\mathbf{b}_{5j} + b_{66}\mathbf{b}_{6j} \right) b_3^3 \right) \mathbf{W} \tag{39c}$$

Where, $\mathbf{b}_{1j}, \ldots, \mathbf{b}_{6j}$ represent first through sixth row of the matrix **B**. Hence, we can write,

$$\mathbf{b}_{1j} = [b_{11} \quad \cdots \quad b_{16}], \cdots, \mathbf{b}_{6j} = [b_{61} \quad \cdots \quad b_{66}] \qquad \text{for } j = 1, 2, \cdots, 6 \tag{40}$$

Using Eq. (21), the virtual twist vector due to flexibility of MS can also be expressed as,

$$\delta \mathbf{S}_{MS} = \mathbf{C}_{MS}\mathbf{W} \tag{41}$$

Where $\mathbf{C}_{MS}$ is called compliance matrix due to flexibility of MS and it can be written in matrix form as,

$$\mathbf{C}_{MS} = \mathbf{B}^T \mathbf{b} \mathbf{B} \tag{42}$$

Where **b** is a 6×6 diagonal matrix and can be written as,

$$\mathbf{b}_{6\times6} = \frac{1}{3E_{MS}I_{MS}} \text{diag}\left(b_1^3, b_1^3, b_2^3, b_2^3, b_3^3, b_3^3 \right) \tag{43}$$

Upon solving the inverse kinematics, the values of b_i and angle λ are calculated. Next matrices **b** and **B** can be obtained. These two matrices along with information on material modulus of elasticity, E_{MS}, and area moment of inertia for MS branches, I_{MS}, will allow us to calculate the compliance matrix due to flexibility of MS, $\mathbf{C}_{MS}$.

3.2.1.2. Obtaining compliance matrix for linear rods (LRs). To calculate the strain energy related to LRs, reaction forces in ith S-joint defined in $\{T_i\}$ are transformed to the local fixed frame $\{B_i\}$. This step will result in two bending components and one axial force at the end of each LR. See Fig. 5. Note that the local fixed coordinate frames $\{B_i\}$, attached to ith S-joint, all have the same direction as the fixed coordinate frame $\{B\}$.

By combining all the reaction forces acting on the S-joints, the original reaction forces can be written as,

$$^T\mathbf{F}_{9\times1} = \left[\begin{array}{ccc} ^{T1}\mathbf{f}_{s1} & ^{T2}\mathbf{f}_{s2} & ^{T3}\mathbf{f}_{s3} \end{array} \right]^T \tag{44}$$

Where $^{Ti}\mathbf{f}_{si} = -\left[f_{ui} \; f_{vi} \; f_{wi} \right]^T$ is the reaction force in ith S-joint defined in its local moving coordinate frame $\{T_i\}$. Also note, the value of f_{ui} for all S-joint is equal to zero. This is because direction of this vector is in line with the direction of the corresponding passive prismatic joint.

Eq. (32) can rewritten as follows,

$$^T\mathbf{F}_{9\times1} = -\mathbf{B}_{9\times6}\mathbf{W}_{6\times1} \tag{45}$$

Where,

$$\mathbf{B}_{9\times6} = \left[\begin{array}{ccccccccc} \mathbf{0} & \mathbf{b}_{1j} & \mathbf{b}_{2j} & \mathbf{0} & \mathbf{b}_{3j} & \mathbf{b}_{4j} & \mathbf{0} & \mathbf{b}_{5j} & \mathbf{b}_{6j} \end{array} \right]^T \qquad \text{for } j = 1, 2, \cdots, 6 \tag{46}$$
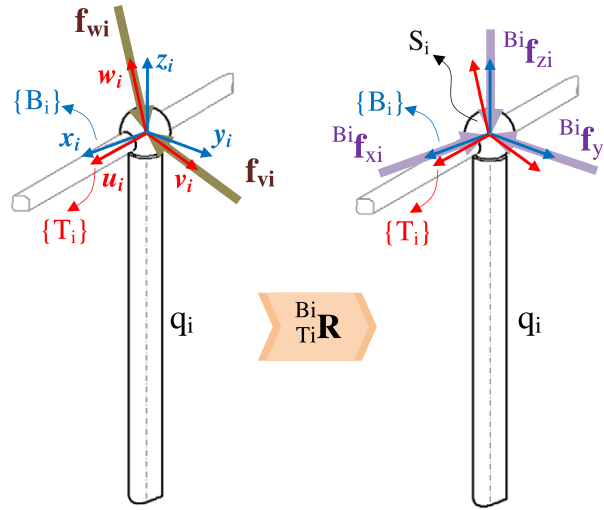
Fig. 5. FBD of the ith linear rod.

Where **0** is a 1×6 zero matrix and $\mathbf{b}_{1j}$ is the first row of matrix **B** (see Eq. (40)). Next, the relationship between the reaction forces in $\{B_i\}$ and the original reaction forces in $\{T_i\}$ can be written as,

$$^B\mathbf{F}_{9\times1} = \mathbf{D}_{9\times9}\,^T\mathbf{F}_{9\times1} \tag{47}$$

Where,

$$^B\mathbf{F}_{9\times1} = [\,^{B1}\mathbf{f}_1 \quad ^{B2}\mathbf{f}_2 \quad ^{B3}\mathbf{f}_3]^T \tag{48}$$

Where $^{Bi}\mathbf{f}_i = [\,^{Bi}\mathbf{f}_{xi} \quad ^{Bi}\mathbf{f}_{yi} \quad ^{Bi}\mathbf{f}_{zi}]^T$ is the reaction force vector that is defined in the fixed local coordinate frame$\{B_i\}$. Further, matrix **D** is defined as,

$$\mathbf{D}_{9\times9} = \mathrm{diag}\left(\begin{bmatrix} ^{B1}_{T1}\mathbf{R} \end{bmatrix} \quad \begin{bmatrix} ^{B2}_{T2}\mathbf{R} \end{bmatrix} \quad \begin{bmatrix} ^{B3}_{T3}\mathbf{R} \end{bmatrix} \right) \tag{49}$$

Where, $^{Bi}_{Ti}\mathbf{R}$ is a rotation matrix which rotates frame $\{T_i\}$ to frame $\{B_i\}$ and is obtained by solving the inverse kinematic. As shown in Fig. 5 and considering Eqs. (45) and (47), the relationship between the external wrench and vector of the reaction forces in S-joints can be written as follows,

$$^B\mathbf{F}_{9\times1} = \mathbf{E}_{9\times6}\mathbf{W}_{6\times1} \quad \rightarrow \quad \mathbf{E}_{9\times6} = -\mathbf{D}_{9\times9}\mathbf{B}_{9\times6} \tag{50}$$

Matrix **E** is called Wrench Compliant Module Jacobian, WMJ$_{LR}$, matrix for the LRs. Note, this matrix maps the applied external wrench on MS to corresponding reaction forces for the compliant module under study, in this case, the LRs. The components of the **E** matrix are referred to as e_{ij}. The internal bending moments, M_{xi} and M_{yi}, as well as the axial force, P_i, in each LR are shown in Fig. 6. Therefore, we can write,

$$M_{xi} = {}^{Bi}f_{yi}\,l_i \qquad \text{for } i = 1, 2, 3 \tag{51}$$

$$M_{yi} = {}^{Bi}f_{xi}\,l_i \qquad \text{for } i = 1, 2, 3 \tag{52}$$

$$P_i = {}^{Bi}f_{zi} \qquad \text{for } i = 1, 2, 3 \tag{53}$$

Strain energy of the three linear rods, U_{LR}, can be written as,

$$U_{LR} = \sum_{i=1}^{3} \int_0^{qi} \left(\frac{P_i^2}{2A_{LR}E_{LR}} + \frac{1}{2E_{LR}I_{LR}}\left(M_{xi}^2 + M_{yi}^2\right) \right) dl_i, \qquad 0 \le l_i \le q_i \tag{54}$$
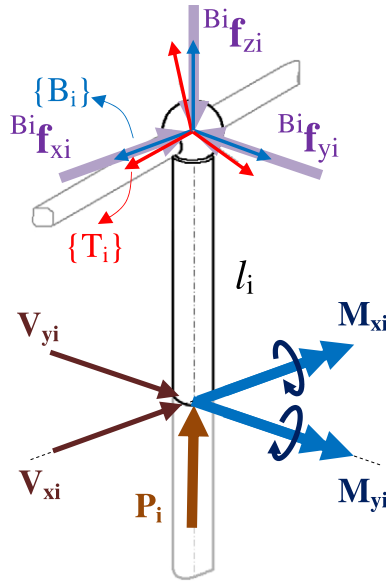
Fig. 6. FBD and section view of the *i*th linear rod.

Where, q_i is the length of *i*th LR and is determined by solving inverse kinematic problem. Using Castigliano's theorem and Eq. (54), the virtual twist vector due to flexibility of LRs, $\delta \mathbf{S}_{LR}$, can be expressed as,

i. Virtual translational displacement of LRs, $\delta \boldsymbol{\chi}_{LR}$

$$\delta \chi_{LRx} = \frac{\partial U_{LR}}{\partial f_x} = \sum_{i=1}^{3} \int_{0}^{qi} \left(\frac{P_i}{A_{LR}E_{LR}} \frac{\partial P_i}{\partial f_x} + \frac{1}{E_{LR}I_{LR}} \left(M_{xi} \frac{\partial M_{xi}}{\partial f_x} + M_{yi} \frac{\partial M_{yi}}{\partial f_x} \right) \right) dl_i \tag{55a}$$

$$\delta \chi_{LRy} = \frac{\partial U_{LR}}{\partial f_y} = \sum_{i=1}^{3} \int_{0}^{qi} \left(\frac{P_i}{A_{LR}E_{LR}} \frac{\partial P_i}{\partial f_y} + \frac{1}{E_{LR}I_{LR}} \left(M_{xi} \frac{\partial M_{xi}}{\partial f_y} + M_{yi} \frac{\partial M_{yi}}{\partial f_y} \right) \right) dl_i \tag{55b}$$

$$\delta \chi_{LRz} = \frac{\partial U_{LR}}{\partial f_z} = \sum_{i=1}^{3} \int_{0}^{qi} \left(\frac{P_i}{A_{LR}E_{LR}} \frac{\partial P_i}{\partial f_z} + \frac{1}{E_{LR}I_{LR}} \left(M_{xi} \frac{\partial M_{xi}}{\partial f_z} + M_{yi} \frac{\partial M_{yi}}{\partial f_z} \right) \right) dl_i \tag{55c}$$

ii. Virtual rotational displacement of LRs, $\delta \boldsymbol{\psi}_{LR}$

$$\delta \psi_{LRx} = \frac{\partial U_{LR}}{\partial M_x} = \sum_{i=1}^{3} \int_{0}^{qi} \left(\frac{P_i}{A_{LR}E_{LR}} \frac{\partial P_i}{\partial M_x} + \frac{1}{E_{LR}I_{LR}} \left(M_{xi} \frac{\partial M_{xi}}{\partial M_x} + M_{yi} \frac{\partial M_{yi}}{\partial M_x} \right) \right) dl_i \tag{56a}$$

$$\delta \psi_{LRy} = \frac{\partial U_{LR}}{\partial M_y} = \sum_{i=1}^{3} \int_{0}^{qi} \left(\frac{P_i}{A_{LR}E_{LR}} \frac{\partial P_i}{\partial M_y} + \frac{1}{E_{LR}I_{LR}} \left(M_{xi} \frac{\partial M_{xi}}{\partial M_y} + M_{yi} \frac{\partial M_{yi}}{\partial M_y} \right) \right) dl_i \tag{56b}$$

$$\delta \psi_{LRz} = \frac{\partial U_{LR}}{\partial M_z} = \sum_{i=1}^{3} \int_{0}^{qi} \left(\frac{P_i}{A_{LR}E_{LR}} \frac{\partial P_i}{\partial M_z} + \frac{1}{E_{LR}I_{LR}} \left(M_{xi} \frac{\partial M_{xi}}{\partial M_z} + M_{yi} \frac{\partial M_{yi}}{\partial M_z} \right) \right) dl_i \tag{56c}$$

Where $\delta \mathbf{S}_{LR} = \begin{bmatrix} \delta \chi_{LRx} & \delta \chi_{LRy} & \delta \chi_{LRz} & \delta \psi_{LRx} & \delta \psi_{LRy} & \delta \psi_{LRz} \end{bmatrix}^T$ is a 6×1 vector. And $\delta \chi_{LRx}, \delta \chi_{LRy} \delta \chi_{LRz}$ and $\delta \psi_{LRx}, \delta \psi_{LRy} \delta \psi_{LRz}$ are components of virtual translational and virtual rotational displacement about x-, y- and z-axes in fixed coordinate frame {B}, respectively. Similar to previous subsection, by substituting the components of **E** matrix into Eqs. (55a–c)–(56a–c), integrating, expanding

and finally factoring the external applied wrench, **W**, we can express the virtual twist vector due to flexibility of linear rods in terms of the applied external wrench. For $j = 1, 2, \cdots, 6$ we can write,

$$\delta\chi_{LRx} = \left(\frac{1}{3E_{LR}I_{LR}}\left(\left(e_{11}\mathbf{e}_{1j} + e_{21}\mathbf{e}_{2j}\right)q_1^3 + \left(e_{41}\mathbf{e}_{4j} + e_{51}\mathbf{e}_{5j}\right)q_2^3 + \left(e_{71}\mathbf{e}_{7j} + e_{81}\mathbf{e}_{8j}\right)q_3^3\right) + \frac{1}{A_{LR}E_{LR}}\left(\left(e_{31}\mathbf{e}_{3j}\right)q_1 + \left(e_{61}\mathbf{e}_{6j}\right)q_2 + \left(e_{91}\mathbf{e}_{9j}\right)q_3\right)\right)\mathbf{W}$$
(57a)

$$\delta\chi_{LRy} = \left(\frac{1}{3E_{LR}I_{LR}}\left(\left(e_{12}\mathbf{e}_{1j} + e_{22}\mathbf{e}_{2j}\right)q_1^3 + \left(e_{42}\mathbf{e}_{4j} + e_{52}\mathbf{e}_{5j}\right)q_2^3 + \left(e_{72}\mathbf{e}_{7j} + e_{82}\mathbf{e}_{8j}\right)q_3^3\right) + \frac{1}{A_{LR}E_{LR}}\left(\left(e_{32}\mathbf{e}_{3j}\right)q_1 + \left(e_{62}\mathbf{e}_{6j}\right)q_2 + \left(e_{92}\mathbf{e}_{9j}\right)q_3\right)\right)\mathbf{W}$$
(57b)

$$\delta\chi_{LRz} = \left(\frac{1}{3E_{LR}I_{LR}}\left(\left(e_{13}\mathbf{e}_{1j} + e_{23}\mathbf{e}_{2j}\right)q_1^3 + \left(e_{43}\mathbf{e}_{4j} + e_{53}\mathbf{e}_{5j}\right)q_2^3 + \left(e_{73}\mathbf{e}_{7j} + e_{83}\mathbf{e}_{8j}\right)q_3^3\right) + \frac{1}{A_{LR}E_{LR}}\left(\left(e_{33}\mathbf{e}_{3j}\right)q_1 + \left(e_{63}\mathbf{e}_{6j}\right)q_2 + \left(e_{93}\mathbf{e}_{9j}\right)q_3\right)\right)\mathbf{W}$$
(57c)

and,

$$\delta\psi_{LRx} = \left(\frac{1}{3E_{LR}I_{LR}}\left(\left(e_{14}\mathbf{e}_{1j} + e_{24}\mathbf{e}_{2j}\right)q_1^3 + \left(e_{44}\mathbf{e}_{4j} + e_{54}\mathbf{e}_{5j}\right)q_2^3 + \left(e_{74}\mathbf{e}_{7j} + e_{84}\mathbf{e}_{8j}\right)q_3^3\right) + \frac{1}{A_{LR}E_{LR}}\left(\left(e_{34}\mathbf{e}_{3j}\right)q_1 + \left(e_{64}\mathbf{e}_{6j}\right)q_2 + \left(e_{94}\mathbf{e}_{9j}\right)q_3\right)\right)\mathbf{W}$$
(58a)

$$\delta\psi_{LRy} = \left(\frac{1}{3E_{LR}I_{LR}}\left(\left(e_{15}\mathbf{e}_{1j} + e_{25}\mathbf{e}_{2j}\right)q_1^3 + \left(e_{45}\mathbf{e}_{4j} + e_{55}\mathbf{e}_{5j}\right)q_2^3 + \left(e_{75}\mathbf{e}_{7j} + e_{85}\mathbf{e}_{8j}\right)q_3^3\right) + \frac{1}{A_{LR}E_{LR}}\left(\left(e_{35}\mathbf{e}_{3j}\right)q_1 + \left(e_{65}\mathbf{e}_{6j}\right)q_2 + \left(e_{95}\mathbf{e}_{9j}\right)q_3\right)\right)\mathbf{W}$$
(58b)

$$\delta\psi_{LRz} = \left(\frac{1}{3E_{LR}I_{LR}}\left(\left(e_{16}\mathbf{e}_{1j} + e_{26}\mathbf{e}_{2j}\right)q_1^3 + \left(e_{46}\mathbf{e}_{4j} + e_{56}\mathbf{e}_{5j}\right)q_2^3 + \left(e_{76}\mathbf{e}_{7j} + e_{86}\mathbf{e}_{8j}\right)q_3^3\right) + \frac{1}{A_{LR}E_{LR}}\left(\left(e_{36}\mathbf{e}_{3j}\right)q_1 + \left(e_{66}\mathbf{e}_{6j}\right)q_2 + \left(e_{96}\mathbf{e}_{9j}\right)q_3\right)\right)\mathbf{W}$$
(58c)

Where, $\mathbf{e}_{1j},\ldots,\mathbf{e}_{9j}$ represent first through ninth row of the matrix **E**. Hence, we can write,

$$\mathbf{e}_{1j} = [e_{11} \cdots e_{16}], \cdots, \mathbf{e}_{9j} = [e_{91} \cdots e_{96}] \qquad \text{for } j = 1, 2, \cdots, 6$$
(59)

Using Eq. (22), the virtual twist vector due to flexibility of LRs can also be expressed as

$$\delta\mathbf{S}_{LR} = \mathbf{C}_{LR}\mathbf{W}$$
(60)

Where, $\mathbf{C}_{LR}$ is called compliance matrix due to flexibility of LRs and it can be written in matrix form as,

$$\mathbf{C}_{LR} = \mathbf{E}^T\mathbf{q}\mathbf{E}$$
(61)

Where, **q** is a 9×9 diagonal matrix and can be written as,

$$\mathbf{q}_{9\times9} = \frac{1}{E_{LR}}\text{diag}\left(\frac{q_1^3}{3I_{LR}}, \frac{q_1^3}{3I_{LR}}, \frac{q_1}{A_{LR}}, \frac{q_2^3}{3I_{LR}}, \frac{q_2^3}{3I_{LR}}, \frac{q_2}{A_{LR}}, \frac{q_3^3}{3I_{LR}}, \frac{q_3^3}{3I_{LR}}, \frac{q_3}{A_{LR}}\right)$$
(62)

Upon solving the inverse kinematics, the values of q_i and angle λ are calculated. Upon these calculations matrices **q** and **E** can be obtained. These two matrices along with information on material modulus of elasticity, E_{LR}, area moment of inertia, I_{LR}, and cross section area, A_{LR}, for LRs will allow us to calculate the compliance matrix due to flexibility of LRs, $\mathbf{C}_{LR}$.

3.2.1.3. Obtaining compliance matrix for motors. To calculate compliance and virtual displacements of the motors, the relationship between axial forces acting at the end of LRs and its resulting motor torque should be found. For this purpose, the ball screw lead and gearbox transmission ratio are used to calculate the resistant torque on the motor. The motor and ball screw assembly are shown in Fig. 7. The relation between ball screw torque and the axial force can be written as follows,

$$\tau_{bi} = \frac{l_b}{2\pi}\left(^{Bi}f_{zi}\right)$$
(63)

Where, τ_{bi} is the resulting ball screw torque due to axial force, $^{Bi}f_{zi}$, on the ith LR. Using gearbox transmission ratio, N, the resistant torque in the motor is,

$$\tau_{mi} = \frac{Nl_b}{2\pi}\left(^{Bi}f_{zi}\right)$$
(64)
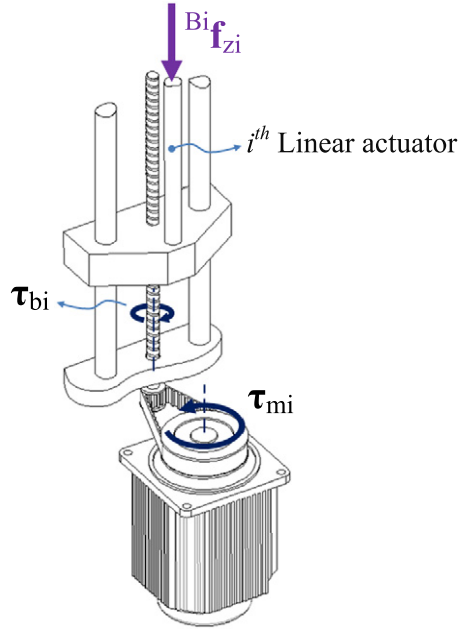
Fig. 7. FBD of the *i*th motor and ball screw assembly.

The gearbox transmission ratio for the 3-PSP is selected to be N = 2. Strain energy of the three motors, U_M, can be written as,

$$U_M = \sum_{i=1}^{3} \left(\frac{\tau_{mi}^2}{2k_{tor,i}} \right) = \frac{N^2 l_b^2}{8\pi^2} \sum_{i=1}^{3} \frac{\left({}^{Bi}f_{zi} \right)^2}{k_{tor,i}} \tag{65}$$

Where $k_{tor,i}$ is equivalent torsional stiffness of ith motor.

Using Castigliano's theorem and Eq. (65), the virtual twist vector due to flexibility of motor, $\delta \mathbf{S}_M$, can be expressed as,

i. Virtual translational displacement of motors, $\delta \boldsymbol{\chi}_M$

$$\delta \chi_{Mx} = \frac{\partial U_M}{\partial f_x} = \frac{N^2 l_b^2}{4\pi^2} \sum_{i=1}^{3} \frac{{}^{Bi}f_{zi}}{k_{tor,i}} \frac{\partial {}^{Bi}f_{zi}}{\partial f_x} \tag{66a}$$

$$\delta \chi_{My} = \frac{\partial U_M}{\partial f_y} = \frac{N^2 l_b^2}{4\pi^2} \sum_{i=1}^{3} \frac{{}^{Bi}f_{zi}}{k_{tor,i}} \frac{\partial {}^{Bi}f_{zi}}{\partial f_y} \tag{66b}$$

$$\delta \chi_{Mz} = \frac{\partial U_M}{\partial f_z} = \frac{N^2 l_b^2}{4\pi^2} \sum_{i=1}^{3} \frac{{}^{Bi}f_{zi}}{k_{tor,i}} \frac{\partial {}^{Bi}f_{zi}}{\partial f_z} \tag{66c}$$

ii. Virtual rotational displacement of motors, $\delta \boldsymbol{\psi}_M$

$$\delta \psi_{Mx} = \frac{\partial U_M}{\partial M_x} = \frac{N^2 l_b^2}{4\pi^2} \sum_{i=1}^{3} \frac{{}^{Bi}f_{zi}}{k_{tor,i}} \frac{\partial {}^{Bi}f_{zi}}{\partial M_x} \tag{67a}$$

$$\delta \psi_{My} = \frac{\partial U_M}{\partial M_y} = \frac{N^2 l_b^2}{4\pi^2} \sum_{i=1}^{3} \frac{{}^{Bi}f_{zi}}{k_{tor,i}} \frac{\partial {}^{Bi}f_{zi}}{\partial M_y} \tag{67b}$$

$$\delta \psi_{Mz} = \frac{\partial U_M}{\partial M_z} = \frac{N^2 l_b^2}{4\pi^2} \sum_{i=1}^{3} \frac{{}^{Bi}f_{zi}}{k_{tor,i}} \frac{\partial {}^{Bi}f_{zi}}{\partial M_z} \tag{67c}$$

Where $\delta \mathbf{S}_M = \begin{bmatrix} \delta \chi_{Mx} & \delta \chi_{My} & \delta \chi_{Mz} & \delta \psi_{Mx} & \delta \psi_{My} & \delta \psi_{Mz} \end{bmatrix}^T$ is a 6×1 vector. Further, $\delta \chi_{Mx}, \delta \chi_{My}, \delta \chi_{Mz}$ and $\delta \psi_{Mx}, \delta \psi_{My}, \delta \psi_{Mz}$ are components of virtual translational and virtual rotational displacement about x-, y- and z-axes in the fixed coordinate frame {B},

respectively. Consider matrix **E** from Eq. (50) and assume $k_{tor, 1} = k_{tor, 2} = k_{tor, 3} = k_{tor}$. Then, by expanding Eqs. (66a–c) and (67a–c) and next factoring the external applied wrench, **W**, the virtual twist vector due to flexibility of motors in terms of the applied external wrench can be obtained. For $j = 1, 2, \cdots, 6$ we can write,

$$\delta\chi_{Mx} = \frac{N^2 l_b{}^2}{4\pi^2 k_{tor}} \left(e_{31}\mathbf{e}_{3j} + e_{61}\mathbf{e}_{6j} + e_{91}\mathbf{e}_{9j} \right)\mathbf{W} \tag{68a}$$

$$\delta\chi_{My} = \frac{N^2 l_b{}^2}{4\pi^2 k_{tor}} \left(e_{32}\mathbf{e}_{3j} + e_{62}\mathbf{e}_{6j} + e_{92}\mathbf{e}_{9j} \right)\mathbf{W} \tag{68b}$$

$$\delta\chi_{Mz} = \frac{N^2 l_b{}^2}{4\pi^2 k_{tor}} \left(e_{33}\mathbf{e}_{3j} + e_{63}\mathbf{e}_{6j} + e_{93}\mathbf{e}_{9j} \right)\mathbf{W} \tag{68c}$$

and,

$$\delta\psi_{Mx} = \frac{N^2 l_b{}^2}{4\pi^2 k_{tor}} \left(e_{34}\mathbf{e}_{3j} + e_{64}\mathbf{e}_{6j} + e_{94}\mathbf{e}_{9j} \right)\mathbf{W} \tag{69a}$$

$$\delta\psi_{My} = \frac{N^2 l_b{}^2}{4\pi^2 k_{tor}} \left(e_{35}\mathbf{e}_{3j} + e_{65}\mathbf{e}_{6j} + e_{95}\mathbf{e}_{9j} \right)\mathbf{W} \tag{69b}$$

$$\delta\psi_{Mz} = \frac{N^2 l_b{}^2}{4\pi^2 k_{tor}} \left(e_{36}\mathbf{e}_{3j} + e_{66}\mathbf{e}_{6j} + e_{96}\mathbf{e}_{9j} \right)\mathbf{W} \tag{69c}$$

Using Eq. (23), the virtual twist vector due to flexibility of motors can be expressed as,

$$\delta\mathbf{S}_M = \mathbf{C}_M\mathbf{W} \tag{70}$$

Where, $\mathbf{C}_M$ is called compliance matrix due to flexibility of the motors and it can be written in matrix form as,

$$\mathbf{C}_M = \mathbf{Q}^T\mathbf{m}\mathbf{Q} \tag{71}$$

Where, **Q** is a 3×6 matrix called Wrench Compliant Module Jacobian, WMJ_M, matrix for the three motors and **m** is a 3×3 diagonal matrix. Matrix **Q** maps the applied external wrench on MS to corresponding resistant torque on the three motors. This matrix can be written as,

$$\mathbf{Q}_{3\times6} = \frac{N l_b}{2\pi} \begin{bmatrix} e_{31} & \cdots & e_{36} \\ e_{61} & \cdots & e_{66} \\ e_{91} & \cdots & e_{96} \end{bmatrix} \tag{72}$$

and,

$$\mathbf{m}_{3\times3} = \frac{N l_b}{2\pi k_{tor}}\mathbf{I}_{3\times3} \tag{73}$$

Where, **I** is 3×3 identity matrix. By adding compliance matrices of the robot compliant modules, and considering Eqs. (24) and (26), the overall stiffness matrix of the 3-PSP parallel robot, **K**, can be calculated. Next, using Eq. (24), we can obtain deflection of the end-effector by applying an external wrench at the MS center. In the next section, results of the two analytical methods are compared with a FEA model and their accuracies are investigated. First, a FEA model of the 3-PSP parallel robot is presented.

4. Finite element analysis

In the previous section, the stiffness matrix of the 3-PSP parallel robot with two analytical methods was presented. In this section, a finite element commercial software is used to evaluate the correctness of the two analytical methods. In the present study, influences of both bending and axial deflection are considered on LRs and MS. For this purpose, element type, BEAM4 is used to develop FEA model for these compliant modules. Furthermore, the cross-sections of these two compliant modules are assumed to be circular. The moving spherical and prismatic joints are assumed rigid and are modeled using MPC184 element type. Each of the three motors is approximated with a linear spring with deformation along z-axis in the fixed coordinate frame {B}. Equivalent stiffness for this linear spring, K_m, determined from Eq. (5), is modeled by COMBIN14 element type. Once the FEA model is developed, it can be used to obtain deflection of the end-effector anywhere within its workspace. However, this requires that the FEA model be re-meshed and re-solved for all points in the workspace [3,13]. This is a highly time consuming process. Therefore, to
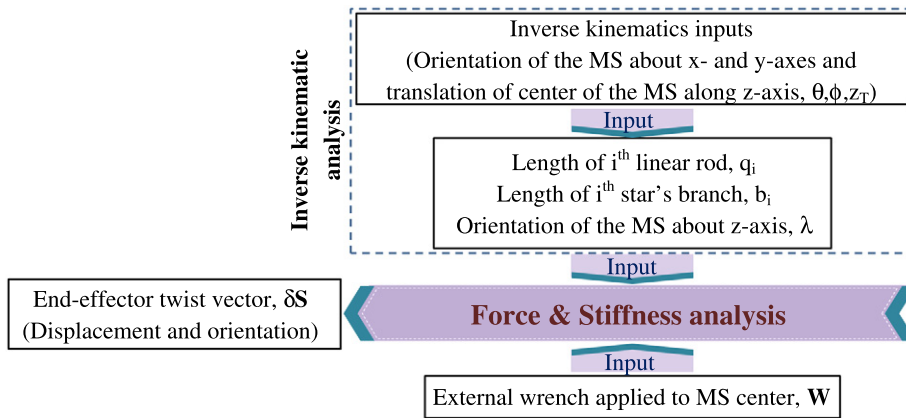
Fig. 8. Stiffness analysis process diagram.

evaluate accuracy of the two analytical results, a few specific points in the workspace are selected. Results are compared with the FEA solutions.

5. FEA and theoretical results — three case studies

The stiffness analysis process is shown in Fig. 8. This figure denotes relation between inverse kinematics and stiffness analysis and their input/outputs.

In manipulators, in addition to physical parameters, stiffness is a function of its configurations. Therefore, it is necessary to first solve inverse kinematics problem before performing stiffness analysis. In this paper, three examples for verifying the theoretical stiffness model of 3-PSP parallel robot are presented. In these examples, first, a desired configuration for the MS, (θ, φ, z_T) is considered. The inverse kinematic is solved and values for essential kinematics parameters of stiffness are obtained. These parameters include, length of MS branches, b_i, length of LRs, q_i, and angle λ, related to MS. Next, an external wrench is applied to the endeffector at point T and twist vector of the end-effector is obtained. To calculate the twist vector of the end-effector in FEA model, a node that coincides with center of MS, point T, is considered. The deflection value of this node depends on applied external wrench and configuration of the MS. Finally, results of FEA model is compared with the two analytical models. The values of the three external wrenches are shown in Table 1. It is assumed that the wrenches are applied to the MS center and are defined in the base coordinate frame {B}.

The physical and architectural parameters of the 3-PSP parallel robot are shown in Table 2. Where "a" denotes the length of vector OA_i (see Fig. 1-c), D_{MS} is diameter of each branch of the MS, E_{MS} and I_{MS} denote elastic modulus and area moment of inertia for each branch of MS, respectively. For LRs, D_{LR} denotes diameter of LR. Furthermore, E_{LR}, I_{LR} and A_{LR} denote elastic modulus, area moment of inertia and cross section area for LR, respectively. Also, l_b is lead of the ball screw and K_{tor} denotes equivalent torsional stiffness of motor.

As stated earlier, three unique positions for the end-effector are considered and inverse kinematic is solved. Results are shown in Table 3.

Table 1
The values of the three external wrenches for the three examples.

Example #1	Example #2	Example #3
${}^B f_{ext} = [200 - 200\ 200]^T$ (N)	${}^B f_{ext} = [200\ 200\ 200]^T$ (N)	${}^B f_{ext} = [0\ 250\ 300]^T$ (N)
${}^B M_{ext} = [75\ 75\ 75]^T$ (N.m)	${}^B M_{ext} = [-75\ 75\ 75]^T$ (N.m)	${}^B M_{ext} = [0\ 150\ 150]^T$ (N.m)

Table 2
Physical and architectural parameter values for the 3-PSP parallel robot.

Parameters	Values	Parameters	Values	Parameters	Values
D_{MS}	0.012 m	D_{LR}	0.02 m	a	0.181 m
$E_{MS} = E_{LR}$	200×10^9 N/m^2	A_{LR}	3.1416×10^{-4} m^2	l_b	0.01 m
I_{MS}	1.0181×10^{-9} m^4	I_{LR}	7.854×10^{-9} m^4	K_{tor}	3×10^5 Nm/rad

Table 3
Inputs/outputs values of inverse kinematic analysis for three configurations.

	Inputs (deg or m)			Outputs (deg or m)								
Parameters	θ	φ	z_T	x_T	y_T	λ	q_1	q_2	q_3	b_1	b_2	b_3
Ex #1	−23	17	0.2	0.002	0.011	−3.48	0.145	0.169	0.302	0.187	0.175	0.217
Ex #2	23	17	0.2	0.002	−0.011	3.48	0.145	0.302	0.169	0.187	0.217	0.175
Ex #3	−28	−12	0.3	0.0086	−0.009	3	0.336	0.188	0.355	0.176	0.223	0.186

Configurations of the 3-PSP parallel robot for the three examples are shown in Fig. 9.

Results of the stiffness analysis are shown in Table 4. This table includes results for the FEA model, the two analytical models and comparison of these results.

The FEA simulation models, for the three examples, with both deformed and un-deformed shapes of the 3-PSP parallel manipulator are shown in Fig. 10.

As shown in Table 4, results of the distributed model and FEA, for all three example, are very close. Furthermore, results of the distributed model are significantly more accurate than the corresponding lumped model. This is because the lumped model disregarded the effect of bending in the compliant modules and assumed MS to be rigid. The distributed model using energy method is clearly advantageous as it eliminates many of the simplifying assumptions. Additionally, the distributed approach allows modeling robot having members with variable cross-sections as well as being under distributed loads. Therefore, in the remaining part of this paper, distributed model is used to obtain the maximum and minimum values of stiffness within a specific part of the workspace as well as the KSI value.

The advantage of the lumped model is its simplicity in deriving the stiffness matrix. Furthermore, if the effect of bending is significant, then, the accuracy of the lumped model can be improved by modeling the bending effect using a torsional spring.
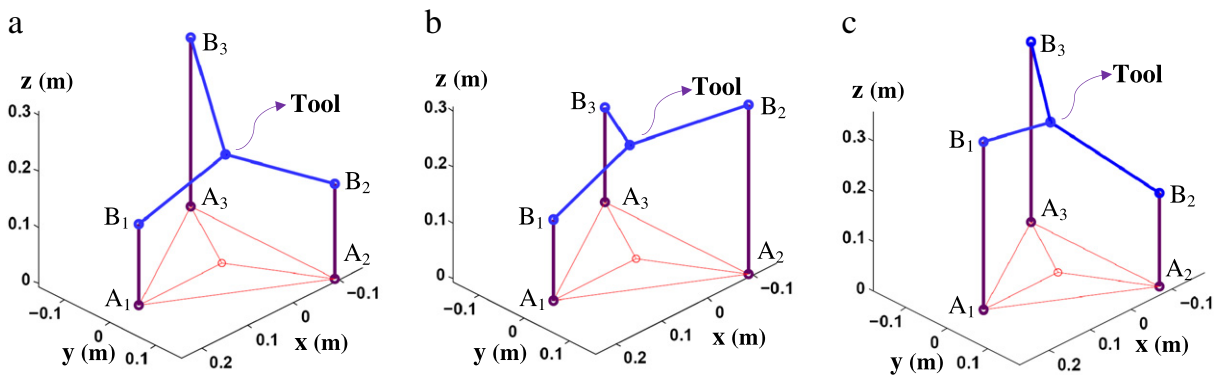
Fig. 9. Result of inverse kinematic analysis, (a) Example #1, (b) Example #2, (c) Example #3.

Table 4
Results of stiffness analysis (comparison between results of FEA and two analytical methods).

	Parameter	Theoretical models $\times 10^{-3}$		FEA result $\times 10^{-3}$		$\|\Delta\|$ with FEA	
		Lumped	Distributed			$\times 10^{-3}$	$\times 10^{-6}$
						Lumped	Distributed
Ex #1	Translation (m)	δx	0.109	3.4456	3.4463	3.34	0.644
		δy	−0.087	−2.9603	−2.9611	2.89	0.801
		δz	−0.003	0.6294	0.6301	63.4	0.688
	Orientation (rad)	$\delta\theta$	0.08	12.598	12.604	12.5	5.97
		$\delta\varphi$	0.15	12.895	12.9	12.7	4.94
		$\delta\lambda$	0.33	10.191	10.193	9.86	2.25
Ex #2	Translation (m)	δx	0.055	2.1901	2.1909	2.14	0.760
		δy	0.031	2.3684	2.3693	2.34	0.915
		δz	−0.0052	0.6068	0.6073	61.2	0.541
	Orientation (rad)	$\delta\theta$	−0.069	−16.0572	−16.066	16.02	8.76
		$\delta\varphi$	0.0718	16.4063	16.416	16.3	9.77
		$\delta\lambda$	−0.025	12.1742	12.183	12.2	8.76
Ex #3	Translation (m)	δx	0.132	0.6905	0.6910	0.56	0.587
		δy	0.0817	1.5688	1.5696	1.49	0.810
		δz	0.0039	1.6999	1.7002	1.7	0.321
	Orientation (rad)	$\delta\theta$	0.0853	8.3907	8.3906	8.3	0.163
		$\delta\varphi$	−0.745	23.0035	23.013	23.1	9.47
		$\delta\lambda$	1.0506	24.117	24.123	23.1	5.66
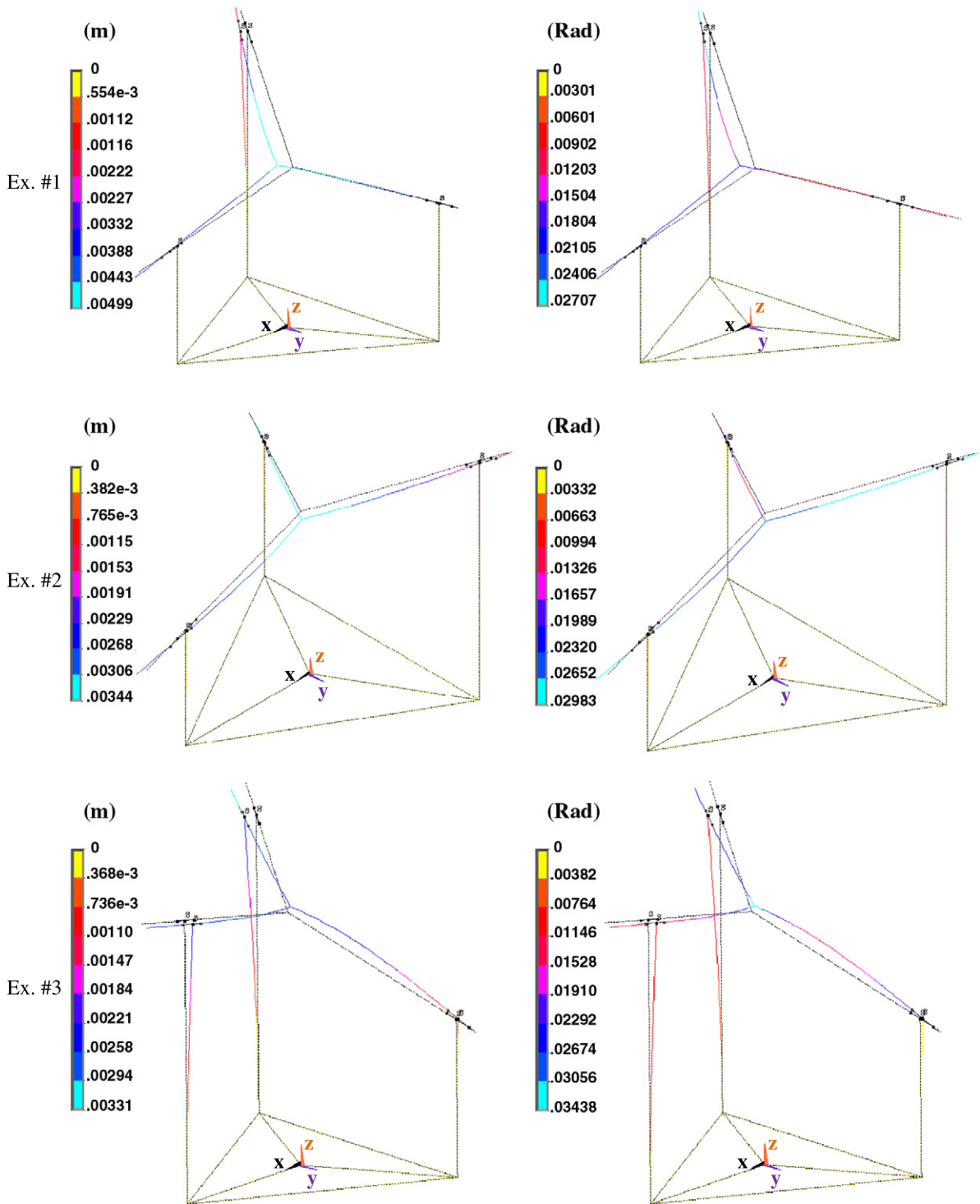
Fig. 10. Translational and rotational displacement contours.

6. Stiffness evaluation of robot in the workspace

In this section, stiffness of the 3-PSP parallel manipulator anywhere in the robot reachable workspace is evaluated. As stated before, stiffness of robot is a function of its configuration and its physical and architectural parameters. One method used to evaluate stiffness is finding the maximum and minimum eigenvalues of stiffness matrix [22,24]. The KSI criterion calculates

the ratio of minimum to maximum eigenvalues of stiffness matrix for any point in the robot workspace [29]. This index is defined as,

$$\mathrm{KSI} = \frac{\sigma_{\min}}{\sigma_{\max}} \tag{74}$$

Where $\sigma_{\min}$ and $\sigma_{\max}$ denote minimum and maximum eigenvalues of stiffness matrix, respectively. In the present work, the more accurate distributed model is used and eigenvalues of the robot stiffness matrix are evaluated. A numerical algorithm for obtaining KSI
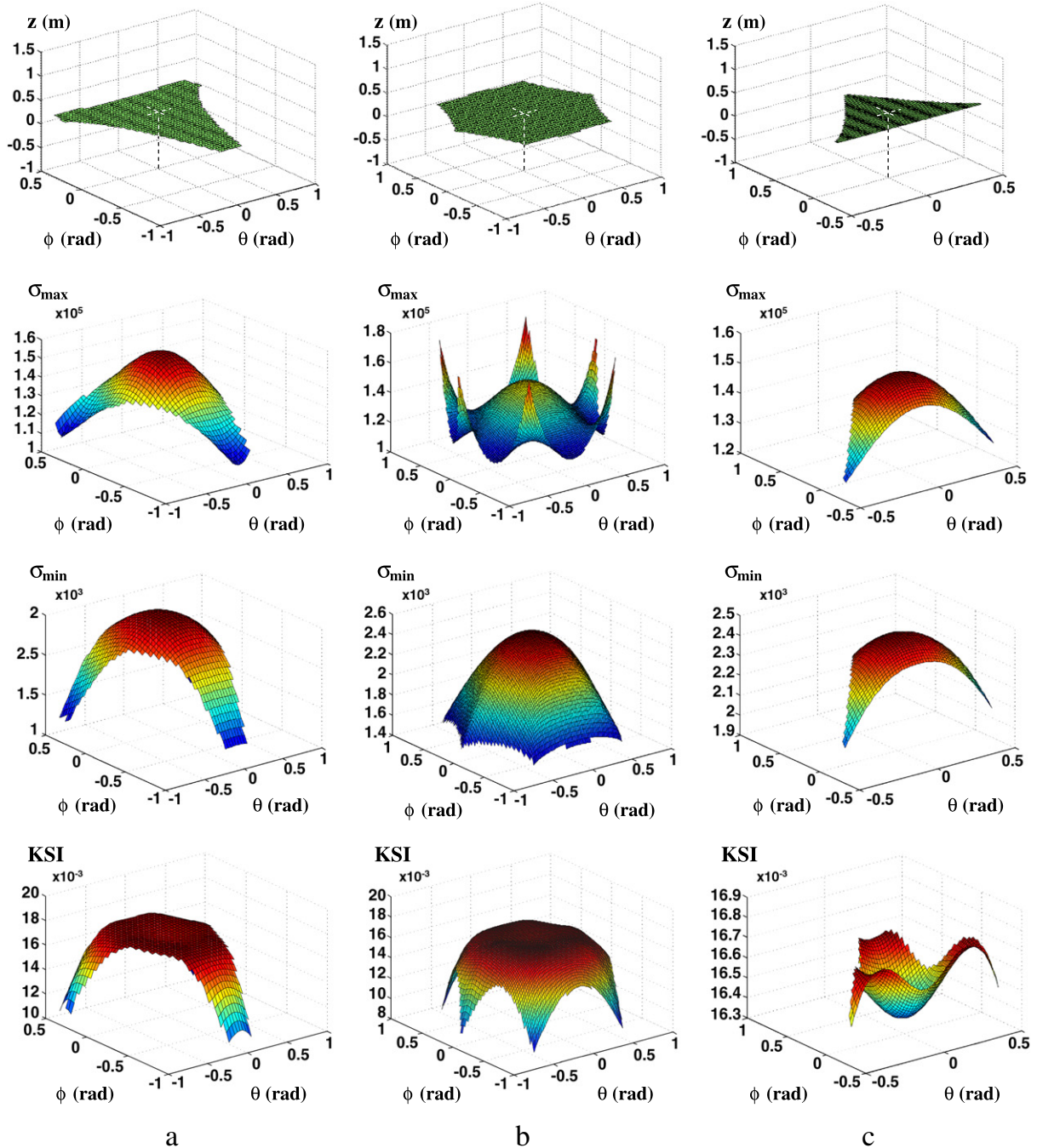
Fig. 11. Workspace, distribution of max and min eigenvalues of stiffness matrix and KSI values. (a) plane z = 0.1 m, (b) plane z = 0.2 m, (c) plane z = 0.35 m in terms of θ and φ.

values in the reachable workspace is developed. First, the reachable workspace for this robot is obtained (see [2] for more details). The z-axis of the 3-PSP robot travels up to 40 centimeters. Therefore, several z planes, ($z = 10$ cm, $z = 20$ cm, $z = 35$ cm) are selected. For each z plane, all different robot configurations, (θ, φ), are considered. For each configuration, six eigenvalues for the 6×6 stiffness matrix are calculated and their maximum and minimum of these values are recorded. The distribution of minimum and maximum eigenvalues of stiffness matrix as well as KSI values for the three planes are illustrated in Fig. 11. As stated earlier, an operator may select any three of the available six DOFs for 3-PSP. This means one may choose the x, y and z location of the end-effector as input to the inverse kinematics problem. Therefore, similar to the θ, φ, z mode, the KSI values for the x, y and z mode are also illustrated in Fig. 12.
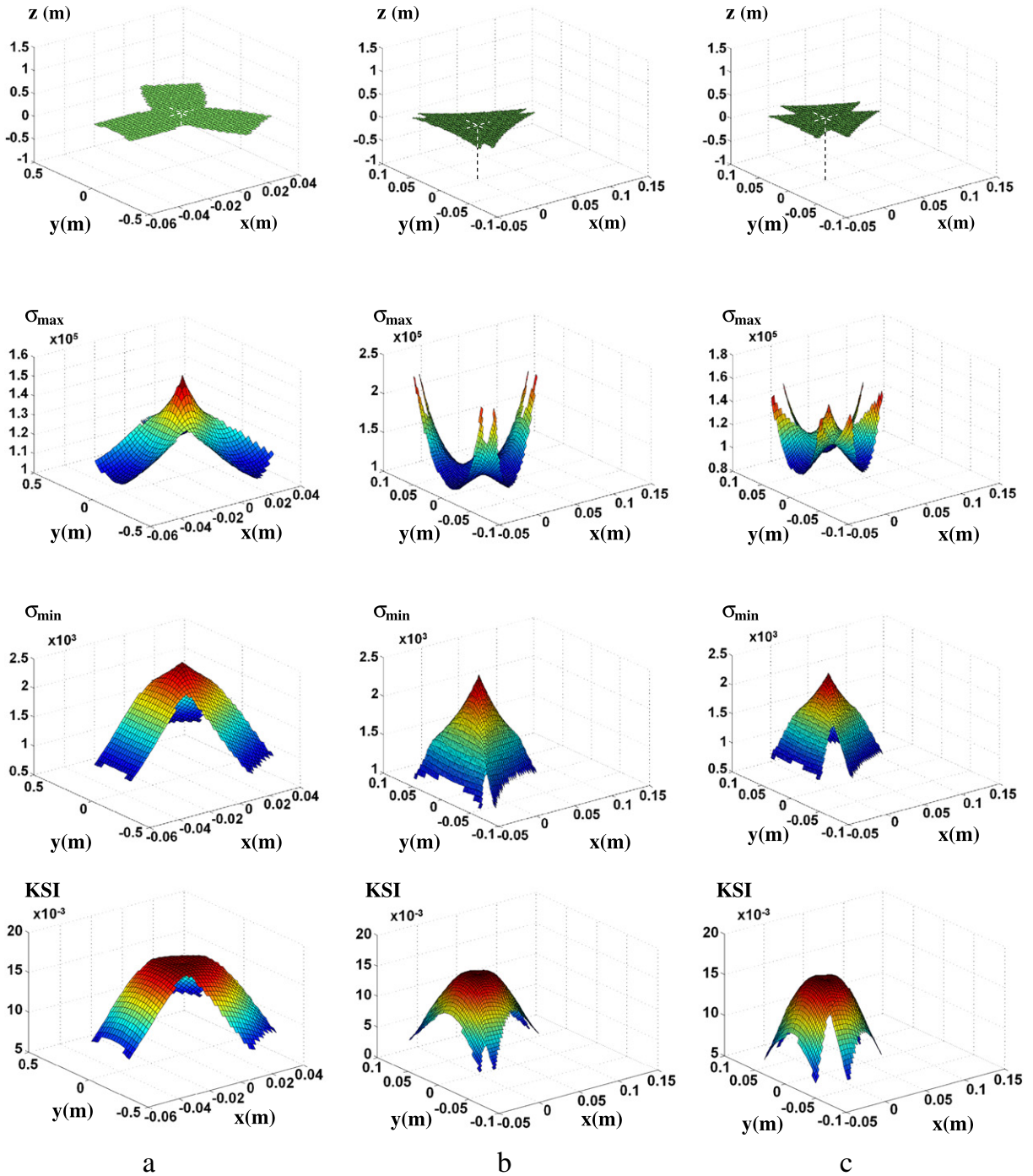
Fig. 12. Workspace, distribution of max/min eigenvalues of stiffness matrix and KSI values. (a) plane $z = 0.1$ m, (b) plane $z = 0.2$ m, (c) plane $z = 0.35$ m in terms of x_T and y_T.

As shown in this figure, in general, as we get closer to the center of the workspace, the stiffness increases and reaches its maximum value at the center.

Figs. 11 and 12 demonstrate that the distributions of stiffness are symmetric. In addition, the stiffness of the 3-PSP parallel robot is best at the center of the workspace and lowest around the boundary of the workspace. Therefore, we should limit or restrict operation of the robot around these boundaries and perhaps other particular subspace of the whole reachable workspace [22]. By choosing proper values for robot structural and material properties, a designer can determine the desired minimum and maximum values for structural stiffness at a specific configuration.

7. Conclusion

In this research, parametric stiffness analysis of a spatial 3-PSP parallel manipulator using three methods, two analytical and one numerical, are presented in details. First, structure of a spatial 3-PSP parallel robot is introduced and closed loop inverse kinematics constraint equations are presented. Next, stiffness analysis is presented using two methods. For the first method, a lumped stiffness model is presented based on principle of virtual work. For this purpose, the overall Jacobian matrix of the robot for determination of the stiffness matrix is introduced. For the second method, an energy approach, a distributed method based on calculation of strain energy of the robot components and Castigliano's theorem is used. Using the energy approach, most simplifying assumptions are eliminated. The moving platform is modeled as flexible and bending effect in major components of the robot is considered. Therefore, the second method provides a much more accurate result. To verify results of the two analytical models, a commercial FEA software is used to model the 3-PSP manipulator. Three numerical examples are provided. Results indicate that the stiffness results of FEA model and the energy approach are very close. This verifies the improved accuracy of the energy approach and suggests that one can depend on such stiffness calculation to estimate stiffness. Furthermore, the energy approach may be used to test alternative designs, specifically link designs, and choose tool trajectories that reduce the tool compliant displacement caused by structural compliance. Finally, by using more accurate analytical method, eigenvalues of stiffness matrix over the workspace are obtained. Using the KSI criterion, the stiffness of robot is evaluated in its workspace and areas where robot is the stiffest are identified. Information about these zones may further be used when considering specific manufacturing requirements. Finally, for each compliant module, a Wrench Compliant Module Jacobian, matrix is introduced which allows mapping the applied external wrench on MS to corresponding reaction forces for the compliant module under study. Once the construction of 3PSP is completed, the experimental study will be performed to validate the results obtained from the stiffness analysis. For our future work, we plan on experimentally validate our theoretical and FEA results.

The main contributions of this paper are the derivation of the stiffness model of a 3-PSP parallel manipulator using two analytical methods, their verification using a commercial FEA model, assumption of flexible moving platform and introduction of the Wrench Compliant Module Jacobian matrix. Other contributions include stiffness evaluation using KSI in workspace. Furthermore, the modeling and analysis methodology presented here use invariant form and can be generalized to other types of parallel manipulators. Lastly, the authors have taken extra care to present the material in this paper in a simplified way with significant details.

References

[1] A. Rezaei, A. Akbarzadeh Tootoonchi, J. Enferadi, Stiffness analysis of a spatial parallel mechanism with flexible moving platform, Proceedings of the ASME, 10th Biennial Conference on Engineering Systems Design and Analysis, Istanbul, (Turkey), 2010.
[2] A. Rezaei, A. Akbarzadeh, M. R. Akbarzadeh T., P. Mahmoodi Nia, Position, Jacobian and Workspace Analysis of a 3-PSP Spatial Parallel Manipulator, Journal of Systems and Control Engineering, IMechE (submitted for publication).
[3] J. Wu, J. Wang, L. Wang, T. Li, Z. You, Study on the stiffness of a 5-DOF hybrid machine tool with actuation redundancy, Mechanism and Machine Theory 44 (2009) 289–305.
[4] A.J. Patel, K.F. Ehmann, Calibration of a hexapod machine tool using a redundant leg, International Journal of Machine Tools and Manufacture 40 (2000) 489–512.
[5] J.S. Chen, W.Y. Hsu, Design and analysis of a tripod machine tool with an integrated Cartesian guiding and metrology mechanism, Precision Engineering 28 (2004) 46–57.
[6] K.H. Harib, A.M.M. Sharif Ullah, A. Hammami, A hexapod-based machine tool with hybrid structure: kinematic analysis and trajectory planning, International Journal of Machine Tools and Manufacture 47 (2007) 1426–1432.
[7] J. Enferadi, A. Akbarzadeh Tootoonchi, Inverse dynamics analysis of a general spherical star-triangle parallel manipulator using principle of virtual work, Nonlinear Dynamic 63 (2010).
[8] H.T. Liu, T. Huang, X.M. Zhao, J.P. Mei, D.G. Chetwynd, Optimal design of the TriVariant robot to achieve a nearly axial symmetry of kinematic performance, Mechanism and Machine Theory 42 (2007) 1643–1652.
[9] Y. Li, Q. Xu, Kinematic analysis of a 3-PRS parallel manipulator, Robotics and Computer-Integrated Manufacturing 23 (2007) 395–408.
[10] D. Kim, W. Chung, Analytic singularity equation and analysis of six-DOF parallel manipulators using local structurization method, IEEE Transactions on Robotics and Automation 15 (4) (1999).
[11] A.B. Koteswara Rao, U. Ravindra Varma, S. Shankar Ganesh, Workspace and stiffness analysis of a two degree of freedom translational parallel kinematic machine, Proceedings of the 2nd International Workshop on Fundamental Research for Parallel Mechanisms and Manipulators, Montpellier (France), 2008.
[12] Q. Xu, Y. Li, An investigation on mobility and stiffness of a 3-DOF translational parallel manipulator via screw theory, Robotics and Computer-Integrated Manufacturing 24 (2008) 402–414.
[13] F. Majou, C. Gosselin, P. Wenger, D. Chablat, Parametric stiffness analysis of the Orthoglide, Mechanism and Machine Theory 42 (2007) 296–311.
[14] S. Li, C. Gosselin, Stiffness analysis of 3-RRR planar parallel mechanisms based on CCT, 12th IFToMM World Congress, Besançon (France), 2007.
[15] S. Son, T. Kim, S.E. Sarma, A. Slocum, A hybrid 5-axis CNC milling machine, Precision Engineering 33 (2009) 430–446.
[16] J.S. Zhao, F. Chu, Z.J. Feng, Symmetrical characteristics of the workspace for spatial parallel mechanisms with symmetric structure, Mechanism and Machine Theory 43 (2008) 427–444.
[17] X.J. Liu, J. Wang, G. Pritschow, Kinematics, singularity and workspace of planar 5R symmetric parallel mechanisms, Mechanism and Machine Theory 41 (2006) 145–169.

[18] K.Y. Tsai, T.K. Lee, K.D. Huang, Determining the workspace boundary of 6-DOF parallel manipulators, Robotica 24 (2006) 605–611.
[19] M. Arsenault, R. Boudreau, Synthesis of planar parallel mechanisms while considering workspace, dexterity, stiffness and singularity avoidance, ASME Journal of Mechanical Design 128 / 69 (2006).
[20] Y.Y. Wang, T. Huang, D.G. Chetwynd, Semi-analytical approach for stiffness estimation of PKM having complex machine frames, 12th IFToMM World Congress, Besançon (France), 2007.
[21] Y. Li, Q. Xu, Kinematics and stiffness analysis for a general 3-PRS spatial parallel mechanism, ROMANSY, Montreal, (Canada), 2004.
[22] Y. Li, Q. Xu, Stiffness analysis for a 3-PUU parallel kinematic machine, Mechanism and Machine Theory 43 (2008) 186–200.
[23] C. Corradini, J.C. Fauroux, Evaluation of a 4-degree of freedom parallel manipulator stiffness, Proceedings of the 11th World Congress in Mechanisms and Machine Science, Tianjin (China), 2003.
[24] J. Enferadi, A. Akbarzadeh Tootoonchi, Accuracy and stiffness analysis of a 3-RRP spherical parallel manipulator, Robotica 29 (2009) 193–209.
[25] J.W. Kim, K.W. Kim, H.S. Kim, J.H. Kyung, "Stiffness analysis and design of a 3-DOF parallel robot with one constraining leg", International Conference on Control, Automation and Systems (2007) 2288–2293.
[26] S. Bhattacharyya, H. Hatwal, A. Ghosh, On the optimum design of Stewart platform type parallel manipulators, Robotica 13 (2) (1995) 133–140.
[27] C.M. Gosselin, Stiffness mapping for parallel manipulators, IEEE Transactions on Robotics and Automation 6 (3) (1990) 377–382.
[28] B.S. El-Khasawneh, P.M. Ferreira, Computation of stiffness and stiffness bounds for parallel link manipulators, International Journal of Machine Tools and Manufacture 39 (1999) 321–342.
[29] C.M. Gosselin, J. Angeles, A global performance index for the kinematic optimization of robotic manipulators, Journal of Mechanical Design 113 (3) (1991) 220–226.
[30] H.K. Jung, C.D. Crane, R.G. Roberts, Stiffness mapping of compliant parallel mechanisms in a serial arrangement, Mechanism and Machine Theory 43 (2008) 271–284.

Glossary

A — Frames

{B}: fixed coordinate frame attached to point O
{T}: moving coordinate frame attached to point T, end-effetor
{B_i}: local fixed coordinate frame attached to point B_i
{T_i}: local moving coordinate frame attached to point B_i

B — Kinematical parameters and vectors

$^B\mathbf{a}_i$: locate corners of the fixed base, A_i, in {B}
$^B\mathbf{q}_i$: position vectors which connect point A_i, to point B_i
$^B\mathbf{b}_i$: position vectors which connect point T to point B_i
$^B\mathbf{T}$: the end-effector position vector defined in {B}.

C — Stiffness parameters for lumped model

K_{ai}: equivalent stiffness value of the ith LR
K_{mi}: equivalent linear spring which models the stiffness of the ith motor
K_{tor}: equivalent torsional stiffness of motor
τ_m: applied moment on motor
$\Delta\theta_m$: rotational deformation of motor
Δq: linear displacement of Nut
l_b: lead of the ball screw
$\mathbf{J}$: the overall Jacobian matrix of the 3-PSP parallel manipulator
$\mathbf{t}$: the MS twist
$\dot{\mathbf{q}}$: the vectors of the linear actuated joint rates
$\delta\mathbf{q}$: virtual infinitesimal displacement vector of LRs
$\boldsymbol{\kappa}_\mathbf{a}$: diagonal matrix consisting of equivalent stiffness of LRs and motors

D — Stiffness parameters for distributed model

$\mathbf{W}$: the applied external wrench
$^B\mathbf{f}_{ext}$: external force vector define in {B}
$^B\mathbf{M}_{ext}$: external moment vector define in {B}
U: total strain energy of manipulator
$\delta\mathbf{S}$: virtual infinitesimal twist vector of the end-effector
$\delta\boldsymbol{\chi}$: virtual translation vector of the end-effector
$\delta\boldsymbol{\psi}$: virtual rotation vector of the end-effector
$\mathbf{C}$: the overall compliance matrix of the 3-PSP parallel manipulator
$\mathbf{K}$: the overall stiffness matrix of the 3-PSP parallel manipulator

   i. Moving Star (MS)

   U_{MS}: strain energy of MS
   $\delta\mathbf{S}_{MS}$: the virtual twist vectors due to flexibility of MS
   $\delta\boldsymbol{\chi}_{MS}$: virtual translation vector due to flexibility of the MS
   $\delta\boldsymbol{\psi}_{MS}$: virtual rotation vector due to flexibility of the MS
   $\mathbf{C}_{MS}$: compliance matrix of the MS
   $^T\mathbf{F}$: reaction forces vector in the S-joints
   f_{ui}: value of reaction force in ith S-joint along u axis
   f_{vi}: value of reaction force in ith S-joint along v axis
   f_{wi}: value of reaction force in ith S-joint along w axis
   $^T\mathbf{v}_i$: the unit vector along the v component of reaction force in {T_i}
   $^T\mathbf{w}_i$: the unit vector along the w component of reaction force in {T_i}
   $\mathbf{B}$: wrench compliant module Jacobian, $WCMJ_{MS}$, matrix for the MS

ii. Linear rods (LRs)

U_{LR}: strain energy of three LRs
$\delta \mathbf{S}_{LR}$: the virtual twist vectors due to flexibility of three LRs
$\delta \boldsymbol{\chi}_{LR}$: virtual translation vector due to flexibility of the LRs
$\delta \boldsymbol{\psi}_{LR}$: virtual rotation vector due to flexibility of the LRs
$\mathbf{C}_{LR}$: compliance matrix of the LRs
$\mathbf{E}$: wrench compliant module Jacobian, $WCMJ_{LR}$, matrix for the LRs

iii. Motors

τ_{bi}: resulting ball screw torque due to axial force on the *i*th LR
τ_{mi}: resistant torque in the motor due to resulting ball screw torque
N: gearbox transmission ratio
U_M: strain energy of three Motors
$\delta \mathbf{S}_M$: the virtual twist vectors due to flexibility of three Motors
$\delta \boldsymbol{\chi}_M$: virtual translation vector due to flexibility of the Motors
$\delta \boldsymbol{\psi}_M$: virtual rotation vector due to flexibility of the Motors
$\mathbf{C}_M$: compliance matrix of the Motors
$\mathbf{Q}$: wrench compliant module Jacobian, $WCMJ_M$, matrix for the Motors

E — Stiffness evaluation

σ_{min}: minimum eigenvalues of the overall stiffness matrix, $\mathbf{K}$
σ_{max}: maximum eigenvalues of the overall stiffness matrix, $\mathbf{K}$